

1 **Measurement report: Enhanced photochemical formation of**
2 **formic and isocyanic acids in urban region aloft: insights**
3 **from tower-based online gradient measurements**

4 Qing Yang^{1,2}, Xiao-Bing Li^{1,2,*}, Bin Yuan^{1,2,*}, Xiaoxiao Zhang^{1,2}, Yibo Huangfu^{1,2}, Lei
5 Yang^{1,2}, Xianjun He^{1,2}, Jipeng Qi^{1,2}, Min Shao^{1,2}

6 ¹ Institute for Environmental and Climate Research, Jinan University, Guangzhou
7 511443, China

8 ² Guangdong-Hongkong-Macau Joint Laboratory of Collaborative Innovation for
9 Environmental Quality, Guangzhou 511443, China

10 * Corresponding authors: Xiao-Bing Li (lixiaobing@jnu.edu.cn), Bin Yuan
11 (byuan@jnu.edu.cn)

12 **Abstract**

13 Formic acid is the most abundant organic acid in the troposphere and has
14 significant environmental and climatic impacts. Isocyanic acid poses severe threats to
15 human health and could be formed through the degradation of formic acid. However,
16 the lack of vertical observation information has strongly limited the understanding of
17 their sources, particularly in urban regions with complex pollutant emissions. To
18 address this issue, we assessed the impact of long tubes on the measurement
19 uncertainties of formic and isocyanic acids and found that the tubing impact was
20 negligible. Then, we conducted continuous (27 days) vertical gradient measurements
21 (five heights between 5-320 m) of formic and isocyanic acids using long tubes based
22 on a tall tower in Beijing, China, in the summer of 2021. Results show that the
23 respective mean mixing ratios of formic and isocyanic acids were 1.3 ± 1.3 ppbv and
24 0.28 ± 0.16 ppbv at 5 m and were 2.1 ± 1.9 ppbv and 0.43 ± 0.21 ppbv at 320 m during the
25 campaign. The mixing ratios of formic and isocyanic acids were substantially enhanced
26 in daytime and correlated with the diurnal change of ozone. Upon sunrise, the mixing
27 ratios of formic and isocyanic acids at different heights simultaneously increased even
28 in the residual layer. In addition, positive vertical gradients were observed for formic
29 and isocyanic acids throughout the day. The positive vertical gradients of formic and
30 isocyanic acids in daytime imply the enhancement of their secondary formation in
31 urban regions aloft, predominantly due to the enhancements of oxygenated volatile
32 organic compounds. Furthermore, the afternoon peaks and positive vertical gradients
33 of formic and isocyanic acids in nighttime also indicate their minor contributions from
34 primary emissions from ground-level sources. The formation pathway of isocyanic acid
35 through $\text{HCOOH}-\text{CH}_3\text{NO}-\text{HNCO}$ was enhanced with height but only accounted for a
36 tiny fraction of its ambient abundance. The abundance and source contributions of
37 formic and isocyanic acids in the atmospheric boundary layer may be highly
38 underestimated when being derived from their ground-level measurements. With the
39 aid of numerical modeling techniques, future studies could further identify key

40 precursors that drive the rapid formation of formic and isocyanic acids, and
41 quantitatively assess the impacts of the enhanced formation of the two acids aloft on
42 their budgets at ground level.

43 **1. Introduction**

44 Formic acid (HCOOH) is the simplest but the most abundant organic acid in the
45 troposphere. It has been widely measured in aqueous (clouds and aerosols) and gaseous
46 phases over urban, rural, and remote regions (*Kawamura and Kaplan, 1983; Chebbi
47 and Carlier, 1996; Kesselmeier et al., 1998; Yu, 2000*). As important contributors to the
48 acidity of precipitation, formic and acetic acids can account for 60% of the free acidity
49 in remote regions (*Galloway et al., 1982; Andreae et al., 1988*), and over 30% of the
50 free acidity in heavily polluted regions (*Keene and Galloway, 1984*). Formic acid is
51 also an important sink of hydroxyl radicals (OH) in clouds (*Jacob, 1986*), playing vital
52 roles in modulating the atmospheric aqueous-phase chemistry through changing pH-
53 dependent reaction rates of related constituents. An in-depth understanding of the
54 concentration levels, spatiotemporal variations, and sources of formic acid is key to
55 elucidating the formation mechanisms of atmospheric secondary pollution. However,
56 the sources and sinks of atmospheric formic acid are still poorly understood so far.

57 There have been many reported sources of atmospheric formic acid. Primary
58 emissions from vegetation activity (*Andreae et al., 1988; Kesselmeier et al., 1998*),
59 microbial metabolism (*Enders et al., 1992*), biomass burning (*Goode et al., 2000*), and
60 vehicle exhaust (*Kawamura et al., 2000*) were identified as important sources of formic
61 acid. Secondary formation from photochemical degradation of volatile organic
62 compounds (VOCs) is another significant source of formic acid (*Khare et al., 1999;
63 Veres et al., 2011; Le Breton et al., 2014; Liggio et al., 2017*). However, current
64 chemical transport models still highly underestimate ambient concentrations of formic
65 acid (*Stavrakou et al., 2011; Paulot et al., 2011; Millet et al., 2015*) and cannot well
66 reproduce its vertical variations. For example, *Mattila et al. (2018)* measured vertical
67 profiles of formic acid using an elevator on the Colorado Front Range BOA tower. They
68 found that formic acid mixing ratios generally decreased with height throughout the day,
69 but there were no known sources to explicitly explain the net surface emissions. In
70 combination with vertical gradient and flux measurements of formic acid in a forest

71 ecosystem, Alwe et al. (2019) suggested that secondary formation, rather than primary
72 emission, is the major source of ambient formic acid. The vertical distribution and
73 variation patterns of formic acid in the atmospheric boundary layer can provide
74 valuable information on the identification and determination of source contributions.
75 Nevertheless, the vertical variations and key drivers of formic acid, particularly in urban
76 regions, are still unclear due to the lack of adequate vertical observations.

77 Isocyanic acid (HNCO) is an inorganic acid and has attracted extensive concerns
78 worldwide in recent years due to its strong toxicity (Wang et al., 2007; Jaisson et al.,
79 2011; Koeth et al., 2013). Previous studies have reported that isocyanic acid is highly
80 soluble at physiological pH and the dissociated cyanate ions (NCO^-) are closely linked
81 to atherosclerosis, cataracts, and rheumatoid arthritis (Mydel et al., 2010; Roberts et al.,
82 2011). At present, there is no standard to clearly define the critical levels of isocyanic
83 acid pollution in ambient air (Rosanka et al., 2020). The mixing ratio of HNCO in the
84 atmosphere exceeding 1 ppbv may endanger human health (Roberts et al., 2011), and
85 the protein carbamylation caused by HNCO in human body may induce various risks
86 (Verbrugge et al., 2015). Similar to formic acid, our understanding of isocyanic acid
87 sources is also very limited.

88 As reported in the literature, primary emissions of isocyanic acid are mainly from
89 combustion sources including cigarette smoke (Hems et al., 2019), gasoline and diesel
90 engine exhausts (Wren et al., 2018), and biomass combustion (Wentzell et al., 2013; Li
91 et al., 2021; Chandra and Sinha, 2016). Wet and dry deposition is known as the main
92 sink of isocyanic acid (Roberts et al., 2014; Rosanka et al., 2020). In addition, isocyanic
93 acid is highly soluble at atmospheric pH and can be hydrolyzed to NH_3 and CO_2 (Zhao
94 et al., 2014; Roberts and Liu, 2019). Secondary formation is another important source
95 of atmospheric isocyanic acid and the known precursors include amides (Barnes et al.,
96 2010), urea (Jathar et al., 2017), and nicotine (Roberts et al., 2011; Borduas et al.,
97 2016). Amides are reported to be the main precursors of isocyanic acid in urban regions
98 (Wang et al., 2020). Isocyanic acid is the oxidative degradation product of amides

99 initiated by OH radicals, NO₃, radicals, and Cl atoms (*Barnes et al., 2010*). In addition
100 to primary emissions from organic solvents and various industrial processes, amides
101 can be also formed through the atmospheric accretion reactions of organic acids with
102 amines or ammonia (*Barnes et al., 2010; Yao et al., 2016*). Vertical gradient
103 measurements of HNCO can help elucidate potential formation sources and
104 mechanisms.

105 Chemical ionization mass spectrometry (CIMS) can effectively detect and
106 quantify atmospheric formic and isocyanic acids (*Bannan et al., 2014; Chandra and*
107 *Sinha, 2016; Liggio et al., 2017; Mungall et al., 2018; Fulgham et al., 2019*). CIMS
108 has been widely used onboard aircraft or on towers to make online vertical
109 measurements of formic and isocyanic acids (*Liggio et al., 2017; Mattila et al., 2018*).
110 Aircraft can carry many types of instruments and achieve measurements of a large suite
111 of parameters (*Benish et al., 2020; Zhao et al., 2021*), but the cost is also very expensive.
112 Towers can provide vertical observations of target species by setting up sites at different
113 heights, building mobile platforms (elevators or baskets) (*Mattila et al., 2018*), and
114 drawing air from multiple heights to the ground-based instruments through long tubes
115 (*Hu et al., 2013; Yáñez-Serrano et al., 2018*). The usage of long tubes is the most
116 convenient and cost-effective method to make gradient measurements of target gaseous
117 species so far. However, interactions between gaseous species and tubing walls may
118 bring unexpected uncertainties for their measurements (*Helmig et al., 2008a; Helmig*
119 *et al., 2008b; Schnitzhofer et al., 2009; Karion et al., 2010; Pagonis et al., 2017*).
120 Therefore, the impacts of long tubing on measurements of formic and isocyanic acids
121 need to be elucidated.

122 In this study, we first assessed the effects of long perfluoroalkoxy (PFA) Teflon
123 tubes on measurements of formic and isocyanic acids. Vertical gradient measurements
124 of the two acids were made through long tubes on a tall tower in urban Beijing, China.
125 Then, the vertical variations and sources of the two acids were investigated and
126 discussed. At last, key conclusions and implications of this study were summarized.

127 **2. Methods and materials**

128 **2.1. Site description and field campaign**

129 Vertical gradient measurements of gaseous species were made on the Beijing
130 Meteorological Tower, which is located on the campus of the Institute of Atmospheric
131 Physics (IAP), Chinese Academy of Sciences. Beijing is the capital city of China with
132 a population of over 20 million by 2020. Beijing has large anthropogenic emission
133 intensities and is suffering from severe air pollution problems (*Acton et al., 2020; Meng*
134 *et al., 2020; Tan et al., 2022*). The tower is located in the northern part of downtown
135 Beijing between the 3rd and 4th Ring Roads and is surrounded by urban roads,
136 expressways, residential areas, restaurants, urban landscaping, and parks. As a result,
137 concentrations of the primary pollutants at the tower site are mainly contributed by both
138 anthropogenic (e.g., vehicular exhausts, cooking, and household volatile chemical
139 products) and biogenic emissions. Detailed descriptions of the tower have been
140 provided in previous studies (*Acton et al., 2020; Yan et al., 2021*) and will not be
141 repeated here. The field campaign was carried out from July 17th to August 3rd, 2021.

142 **2.2. Instrumentation**

143 To obtain online gradient measurements of atmospheric trace gases, we
144 established a tower-based observation system using a combination of online
145 measurement techniques and long tubes (Figure S1). The system and related
146 assessments on the usage of long tubes have been explicitly described in our previous
147 study (*Li et al., 2023*) and will be briefly introduced here. After removing fine particles
148 by PFA Teflon filters (Whatman) with a diameter of 46.2 mm and a pore size of 2 μm ,
149 ambient air at four altitudes on the tower (namely 47, 102, 200, and 320 m) was
150 simultaneously and continuously drawn to the ground through long PFA Teflon tubes
151 (100, 150, 250, and 400 m; outer diameter: 1/2"; inner diameter: 0.374") by a vacuum
152 pump. The flow rate of the sample stream in each tube was controlled by a critical
153 orifice and ranged between 13-21 standard liters per minute (SLPM), as shown in table

154 S1. The flow rates in long tubes were retained as large as possible if instruments allowed
155 to minimize the impact of gas-surface interactions on measurements of targeted gaseous
156 species (*Deming et al., 2019; Li et al., 2023*). Two air-conditioned containers were
157 placed next to each other on the base of the tower and all the instruments were operated
158 inside. An additional inlet of the tube was mounted on the rooftop of the container
159 (approximately 5 m above ground level) to make measurements of trace gases near the
160 surface. Therefore, the tower-based observation system consisted of five inlet heights
161 ranging from the ground level to 320 m. Inlets of the instruments were connected to the
162 outlet of a Teflon solenoid valve group, which was used to perform the switch of the
163 inlet heights at time intervals of 4 minutes. Vertical gradient measurements of gaseous
164 species were cyclically made over periods of 20 minutes. Indoor PFA Teflon tubes were
165 wrapped with insulation tubes and were heated to prevent condensation of water and
166 organic gases.

167 Formic and isocyanic acids were measured by a high-resolution time-of-flight
168 chemical ionization mass spectrometry with iodide reagent ion (ToF-CIMS). Due to the
169 high sensitivity to oxygenated volatile organic compounds (OVOCs), the iodine ion
170 source has been widely used in previous studies (*Yuan et al., 2015; Schobesberger et*
171 *al., 2016; Mungall et al., 2018*). A Filter Inlet for Gases and AEROSols (FIGAERO)
172 was used to perform the switch between the gas and particle measurement modes
173 (*Lopez-Hilfiker et al., 2014*). The ion molecular reaction (IMR) chamber is adjacent to
174 the FIGAERO and utilizes a vacuum ultraviolet ion source (VUV-IS). Iodide anion (I^-)
175 is produced from the photoionization of methyl iodide (CH_3I) in IMR (*Ji et al., 2020*).
176 During the measurements, I^- was produced by introducing the CH_3I gas standard (1000
177 ppm, Dalian Special Gases, China) to the IMR chamber at a flow rate of 2 standard
178 cubic centimeters per minute (SCCM) in 200 SCCM high-purity nitrogen (N_2 ,
179 99.9995%) by the VUV-IS. The pressure of the IMR chamber was maintained at 70-80
180 mbar. Flow rates of the sample gas were maintained at 2 SLPM using a critical orifice.
181 During the field campaign, both gaseous and particle measurements were made through

182 the FIGAERO of the CIMS, but only gaseous measurements were analyzed in this study.
183 In a one-hour cycle, the first 24 min was allocated to make gaseous measurements
184 during which a complete vertical profile of a gaseous species can be obtained. In the
185 gaseous measurement mode, a rapid blank measurement was made for 10 s at 3-min
186 intervals in the first 21 min and a long-time blank measurement was made in the rest 3
187 min (*Palm et al., 2019*). During the first 21-min period of the one-hour cycle, another
188 inlet at 5 m was used to collect ambient particles using PTFE membrane filters
189 (Zefluor®, Pall Inc., USA). Therefore, the remaining 36 min of the one-hour cycle was
190 allocated to analyze the collected particle.

191 Calibrations of the ToF-CIMS for formic and isocyanic acids were performed in
192 the laboratory before and after the field campaign. Standard solutions of formic acid
193 were evaporated using the liquid calibration unit (LCU, IONICON Analytik GmbH)
194 and then diluted to designated concentration gradients by being mixed with zero air at
195 five flow rates. The gas standard of isocyanic acid is unstable at ambient temperature
196 and thus no commercial gas cylinder was available. Instead, cyanuric acid solution was
197 put into a diffusion cell and heated to 300 °C to generate isocyanic acid gas at a stable
198 mixing ratio. An ion chromatograph was used to quantify the concentration of the gas
199 standard by measuring deionized water that absorbed the isocyanic acid gas. Detailed
200 information about the isocyanic acid calibration procedure has been provided in our
201 previous work (*Wang et al., 2020*). Impacts of the changes in ambient humidity on
202 measurements of the ToF-CIMS for both formic and isocyanic acids were determined
203 in the laboratory and were corrected when calculating their respective concentrations.
204 Measured signals of the ToF-CIMS were processed using the Tofware software package
205 (version 3.0.3; Tofwerk AG, Switzerland).

206 A high-resolution proton-transfer-reaction quadrupole interface time-of-flight
207 mass spectrometry (PTR-ToF-MS) with both H_3O^+ and NO^+ ion chemistry was used to
208 measure reported precursors of the two acids, such as isoprene, aromatics, OVOCs, and
209 amides. Detailed information about the configuration and operation setup of the PTR-

210 ToF-MS has been provided in our previous studies (*Yuan et al., 2017; Wu et al., 2020;*
211 *Li et al., 2022*). Mixing ratios of O₃, CO, and NO₂ were measured by a UV absorption
212 O₃ analyzer (T400, Teledyne API, USA), a gas filter correlation CO analyzer (T300,
213 Teledyne API, USA), and a trace level NO_x analyzer (42i, Thermos, USA), respectively.
214 Photolysis rates were measured by a PFS-100 photolysis spectrometer (Focused
215 Photonics Inc.) on the rooftop of the container. The planetary boundary layer height
216 (PBLH) data was obtained from the website of the Air Resources Laboratory
217 (<https://ready.arl.noaa.gov/READYamet.php>). Measurements of isocyanic acid and
218 amides made in Guangzhou and Gucheng in China were also used in this study for
219 comparison, and more information about these observations can be found in our
220 previous papers (*Wang et al., 2020*).

221 **2.3. Tubing assessment**

222 The tower-based observation system used long PFA Teflon tubes (hundreds of
223 meters in length) to draw air samples from different heights. The interactions between
224 tubing inner walls and organic compounds, namely the absorption/desorption of trace
225 gases, have nonnegligible impacts on their measurements after traversing such long
226 tubes (*Pagonis et al., 2017; Deming et al., 2019*). The equilibrium between the
227 absorption and desorption of organic compounds on tubing walls required distinct times,
228 namely tubing delay, for different species. For nonpolar/weak-polar organic compounds,
229 their tubing delays and measurement uncertainties after traversing long tubes are
230 dependent on their saturation concentrations and the flow rates of sample streams but
231 are independent of changes in humidity (*Krechmer et al., 2017; Pagonis et al., 2017*).
232 For some small polar organic compounds, their tubing delays and measurement
233 uncertainties after traversing long tubes are dependent on Henry's law coefficients and
234 are affected by changes in humidity (*Liu et al., 2019*). The performance of long PFA
235 Teflon tubes in measuring concentrations of nonpolar/weak-polar organic compounds
236 and inorganic species (e.g., ozone, NO, NO₂, and CO₂) has been assessed in our
237 previous work (*Li et al., 2023*). The impacts of long PFA Teflon tubes on measurements

238 of formic and isocyanic acids are still unclear and will be assessed in this study.

239 Long PFA Teflon tubes with an outer diameter of 1/2" and an inner diameter of
240 0.374" were used to draw air samples from different altitudes and thus were assessed.
241 At flow rates below 20 SLPM, suitable pressure drops can be maintained in these long
242 tubes for instrument operation (*Li et al., 2023*). The effects of long tubes on
243 measurements of formic and isocyanic acids were mainly assessed using the same
244 methods in the literature (*Li et al., 2023*). The tubing delay of formic acid is estimated
245 as the time required to reach 90% of the concentration change made at the tubing inlet.
246 The depassivation curve of formic acid measured at the air outlet end of the tubing was
247 used to calculate its tubing delay and was obtained by using a step-function change in
248 its concentration at the tubing inlet (*Pagonis et al., 2017; Deming et al., 2019*). The
249 formic acid signals were normalized to those measured at the beginning of the step-
250 function change and then were fitted using the double exponential method, as shown in
251 Figure 1. Finally, the tubing delay of formic acid was determined when the fitting line
252 decreased to 0.1. The previous study (*Li et al., 2023*) has reported that inorganic species
253 have small tubing delays even in a 400 m long tube. Therefore, tubing delays of
254 isocyanic acid in long tubes are not discussed in this study.

255 To further assess the impacts of long tubes (namely 100, 200, 300, and 400 m)
256 on measurements of formic and isocyanic acids in real environments, their ambient
257 mixing ratios measured through different lengths of tubes were intercompared by
258 running the inlets side by side at ground level. Ambient air samples were sequentially
259 drawn with and without the tubes through a Teflon solenoid valve group (Figure S2),
260 which was set to perform the switch at time intervals of 4 minutes. Instrument
261 backgrounds of the two species were measured for 10 s at time intervals of 1 minute by
262 passing zero air into the instrument at a flow rate of 3 SLPM. Inter-comparisons of the
263 formic acid and isocyanic acid measurements made through different lengths of tubes
264 were mainly performed using linear fittings ($y=kx+b$; k is the slope and b is the
265 intercept).

266 **3. Results and Discussions**

267 **3.1. Interactions between long tubes and the two acids**

268 As shown in Figure 1, signals of formic acid measured by the ToF-CIMS had a
269 tubing delay of 23 s after traversing the 400 m long tube at the flow rate of 13 SLPM.
270 In addition to the interactions between tubing walls and formic acid molecules (*Pagonis*
271 *et al.*, 2017; *Deming et al.*, 2019), molecular diffusion and dispersion (namely Taylor
272 dispersion) can cause the longitudinal mixing of gas molecules in the tubing and is also
273 an important factor contributing to the measured delays (*Karion et al.*, 2010). Molecular
274 diffusion and dispersion have strong dependences on molecular diffusion coefficients
275 and tubing flow rates (*Karion et al.*, 2010). The influential time of Taylor dispersion on
276 the measurements of formic acid through a 400 m long tube at the flow rate of 13 SLPM
277 was estimated to be only 2.9 s, which is much smaller than the measured tubing delay
278 (23 s) of formic acid. Therefore, the adsorption/desorption of formic acid molecules on
279 tubing inner walls plays a dominant role in determining the tubing delay.

280 For most organic compounds, the tubing delays generally depend on tubing flow
281 rates and their saturated concentrations (C^*) (*Li et al.*, 2023; *Deming et al.*, 2019). With
282 the increase in tubing length and flow rate, the tubing delays of organic compounds will
283 rapidly decrease (*Liu et al.*, 2019). Therefore, the tubing flow rates should be as large
284 as possible if the instrument could work normally. In addition, the tubing delays of
285 organic compounds generally increase with the decrease in their C^* (*Li et al.*, 2023). It
286 must be acknowledged that tubing delay is inevitable. The analysis time scales of
287 species concentrations measured through long tubes should be greater than their tubing
288 delays, especially for those with small C^* .

289 As shown in Figure S3(a), ambient mixing ratios of formic acid measured
290 through the 400 m long tube varied consistently with those measured without the tube
291 with mean values of 4.14 and 4.09 ppbv, respectively. The mixing ratios of formic acid
292 measured with the long tube were slightly higher in the daytime and lower at night in

293 comparison with those measured without the long tube. We also conducted a correlation
 294 analysis between the mixing ratios of formic acid measured with and without long tubes.
 295 As shown in Figure 2, the mixing ratios of formic acid measured with and without the
 296 400 m long tube agreed within 20%, but the slope of the linear fitting ($k=0.84$) is lower
 297 than 1. The differences of formic acid mixing ratios measured with and without the 400
 298 m long tube were predominantly caused by the long-tail memory effect of the tubing
 299 (Figure 1). For example, the mixing ratios of formic acid measured through the 400 m
 300 long tube at night equaled to its ambient mixing ratios plus those released from the
 301 tubing inner wall. The tubing delay of formic acid was determined when its mixing
 302 ratios reached 90% of the change before entering the tubing. However, the long-tail
 303 memory effect of the tubing mainly focused on the rest 10% of the change (Figure 1),
 304 which required a much longer time to stabilize.

305 Impacts of the tubing memory effects will be accumulated due to the continuous
 306 change in ambient concentrations of formic acid. To further assess the impacts of tubing
 307 memory effects on measurement uncertainties of the two acids, differences between
 308 mixing ratios of the species X (namely formic and isocyanic acids) measured with and
 309 without long tubes at time t (denoted by $\delta[X]_t$) were calculated using Eq. (1):

$$310 \quad \delta[X]_t = [X_{without}]_t - [X_{with}]_t \quad (1)$$

311 where $[X_{with}]_t$ and $[X_{without}]_t$ refer to mixing ratios of the species X measured at
 312 time t with and without long tubes, respectively; Δt is the change in time relative to
 313 time t and was used to characterize the influential time of the memory effect. In addition,
 314 the changes in mixing ratios of the species X measured using long tubes at time t relative
 315 to its average mixing ratio over the previous time interval of Δt (denoted by $\Delta[X]_t$)
 316 was also calculated using Eq. (2):

$$317 \quad \Delta[X]_t = [X_{with}]_t - \frac{\sum_{t-\Delta t}^t [X_{with}]}{\Delta t} \quad (2)$$

318 A strong correlation between $\delta[X]_t$ and $\Delta[X]_t$ could be captured at a certain Δt if
 319 the tubing memory effect make essential contributions to measurement uncertainties of
 320 the species X after traversing long tubes. For the 400 m long tubing, $\delta[X]_t$ and $\Delta[X]_t$

321 had the strongest correlation ($R^2=0.89$) when Δt was approximately 14 h (Figure S5).
322 As also shown in Figure 2(a), the mixing ratios of formic acid measured with and
323 without the 400 m long tube agreed well when $\Delta[HCOOH]$ approached to zero. The
324 decrease and increase in $\Delta[HCOOH]$ will enlarge measurement uncertainties of formic
325 acid using the long tube. In morning periods, ambient mixing ratios of formic acid
326 rapidly increased. As a result, the mixing ratios of formic acid measured through the
327 400 m long tube were slightly lower than its ambient mixing ratios due to the absorption
328 of formic acid by tubing inner walls. In evening and nighttime periods, an opposite
329 phenomenon was observed due to the desorption of formic acid from tubing inner walls
330 (Figure S3). In addition to the 400 m long tube, impacts of the tubes with lengths of
331 100, 200, and 300 m on measurements of formic acid were also assessed, as shown in
332 Figures 2(c) and 3(a). The usage of tubes with lengths of 100, 200, and 300 m has
333 negligible impacts on the measurements of formic acid.

334 In contrast to formic acid, the usage of long tubes had minor impacts on the
335 measurements of isocyanic acid. The mixing ratios of isocyanic acid measured with and
336 without the 400 m long tube varied consistently ($k=0.86$, $R^2=0.90$) with mean values of
337 0.25 and 0.26 ppbv, respectively (Figure S3). As shown in Figure 2(b), $\Delta[HNCO]$ is
338 evenly distributed on both sides of the 1:1 line. Therefore, the changes in ambient
339 concentrations of isocyanic acid do not have significant impacts on the measurements
340 of isocyanic acid through the long tubes. As also shown in Figure 3(b), $\delta[HNCO]$ and
341 $\Delta[HNCO]$ of isocyanic acid were independent of the changes in isocyanic acid mixing
342 ratios. The R^2 values of linear fittings were less than 0.21 for the isocyanic acid
343 measurements made using different lengths of tubes. This is consistent with the results
344 reported in the literature (*Helmig et al., 2008a; Helmig et al., 2008b; Li et al., 2023*)
345 that inorganic species with low reactivities can be well measured using long PFA Teflon
346 tubes. The test results confirm that the measurements of formic and isocyanic acids
347 made through long tubes can be used to characterize their vertical and temporal
348 variations.

349 **3.2. Vertical variations and sources of formic acid**

350 Time series of formic acid and ozone mixing ratios at 5 and 320 m are shown in
351 Figure 4. The concentrations of formic acid and ozone exhibited similar diurnal and
352 inter-diurnal variations at different altitudes during the campaign. Hourly mean mixing
353 ratios of ozone exhibited strong temporal variations with an average of 43.5 ± 25.3 ppbv
354 at 5 m and an average of 53.5 ± 25.0 ppbv at 320 m. Hourly mean mixing ratios of formic
355 acid at 5 m ranged between 0.1-6.6 ppbv with an average of 1.3 ± 1.3 ppbv at 5 m, which
356 is comparable to those observed in other megacities, such as Shenzhen (1.2 ppbv) in
357 China (*Zhu et al., 2019*), London (1.3 ppbv) in UK (*Bannan et al., 2017*), and Los
358 Angeles (2.0 ppbv) in USA (*Yuan et al., 2015*). By contrast, hourly mean mixing ratios
359 of formic acid at 320 m had an average of 2.1 ± 1.9 ppbv, approximately 1.6 times higher
360 than that at 5 m. The temporal variability of formic and isocyanic acids were mainly
361 caused by the diurnal and inter-diurnal changes in meteorological conditions (e.g., solar
362 radiation and PBLH).

363 Before July 12th, the daily maximum hourly mixing ratios of ozone at 5 m all
364 exceeded 100 ppbv, indicating the enhanced formation of secondary air pollutants
365 associated with photochemical reactions. The mixing ratios of formic acid measured
366 before July 12th were also prominently larger than those measured after, suggesting
367 important contributions from photochemical formations. The photochemical formation
368 of secondary pollutants was weak from July 13th to 30th due to the cloudy and rainy
369 weather. After August 1st, low mixing ratios of ozone and formic acids were observed
370 along with the occurrence of favorable dilution conditions characterized by high PBLHs.

371 As shown in Figure 5, the mixing ratios of formic acid measured at the five
372 altitudes (namely 5, 47, 102, 200, and 320 m) exhibited similar diurnal patterns. After
373 sunrise (~6:00 LT), formic acid mixing ratios increased rapidly at each altitude before
374 reaching the peak between 14:00-16:00 LT and then continuously declined before
375 sunrise the following day. Similar diurnal variation patterns of formic acid were also
376 observed at other urban sites (*Veres et al., 2011*), rural sites (*Hu et al., 2022*), and remote

377 sites (*Schobesberger et al., 2016*). The diurnal variation patterns of formic acid were
378 highly similar to those of ozone (a typical secondary pollutant) but were different from
379 those of VOCs from primary emissions. Taking toluene as an example, toluene is a
380 typical VOC tracer of anthropogenic emission sources in urban regions, such as
381 industrial processes and vehicular exhausts (*Fang et al., 2016; Skorokhod et al., 2017*),
382 and is also an important precursor of ozone (*Yuan et al., 2012*). The mixing ratios of
383 toluene exhibited opposite diurnal variation patterns to those of ozone and formic acids
384 with the minima occurring at around 14:00 LT. The lower mixing ratios of toluene in
385 daytime than in nighttime were predominantly caused by the enhancement of
386 atmospheric dilution and chemical removal by OH radicals (*De Gouw et al., 2018*). The
387 mixing ratios of formic acid poorly correlated (R^2 ranged between 0.16-0.28) with those
388 of CO (a typical tracer of combustion sources) at the five altitudes but well correlated
389 (R^2 ranged between 0.67-0.75) with those of Ox (O_3+NO_2 , a conserved metric of ozone
390 by removing NO titration effect), as shown in Figure 6. These results further confirm
391 that ambient concentrations of formic acid in urban Beijing were dominantly
392 contributed by secondary sources associated with photochemical reactions rather than
393 primary emissions.

394 Another observed evidence for the dominant contribution of formic acid from
395 secondary formations is its positive vertical gradients in nighttime (defined as the
396 period of 22:00-5:00 LT), as shown in Figure 7. Large amounts of formic acid will
397 accumulate near the surface with strong negative vertical gradients if primary emissions
398 dominate its contributions, as manifested by vertical toluene profiles. At nighttime, the
399 mixing ratios of ozone also increased with height due to enhanced removal by NO
400 titration and surface dry deposition. The deposition of formic acid was also enhanced
401 near the surface, driving the formation of positive gradients in vertical formic acid
402 profiles.

403 A notable difference existed between the diurnal variation patterns of ozone and
404 formic acid above the ground. As shown in Figure 5, the mean mixing ratios of ozone

405 at 5 m rapidly increased from 21.5 ppbv to 36.0 ppbv from 6:00 to 10:00 LT, while the
406 mean mixing ratios of ozone at 320 m slightly increased from 16.3 ppbv to 16.9 ppbv
407 during the same period. The enhancement rate is defined as the average change rate of
408 the species concentration between two adjacent hours. As shown in Figure 8, the
409 enhancement rates of ozone mixing ratios between 6:00 and 10:00 LT decreased with
410 the increase in height. This phenomenon indicates relatively weak photochemical ozone
411 formation in urban regions aloft before 10:00 LT due to the lack of reactive ozone
412 precursors (e.g., unsaturated hydrocarbons and NO_x). With the enhancement of the
413 vertical exchange of air masses with the rise of the boundary layer, large amounts of
414 ozone precursors (e.g., the observed peaks of toluene mixing ratios at 320 m at 10:00
415 LT) emitted from surface sources were transported upward and drove the formation of
416 ozone in high altitudes. In contrast to ozone, the mixing ratios of formic acid at the five
417 altitudes all increased rapidly between 6:00 and 10:00 LT. The enhancement rate of
418 formic acid mixing ratios between 6:00 and 10:00 LT kept nearly constant below 320
419 m (Figure 8). This result implies that the oxidation products of VOCs over nighttime or
420 in the daytime before are important precursors of formic acid and can drive the rapid
421 formation of formic acid with further photooxidation. This speculation can be supported
422 by the vertical and diurnal variations of methyl vinyl ketone (MVK), methacrolein
423 (MACR), and formaldehyde, which are reported key precursors of formic acid as shown
424 in Figure 5(d) and 5(e). The diurnal variation patterns of MVK+MACR and
425 formaldehyde at the five latitudes were nearly the same with the enhancements in
426 daytime. In addition, concentrations of MVK+MACR and formaldehyde all increased
427 with height in nighttime and early morning periods, facilitating the photochemical
428 formation of formic acid even in the residual layer.

429 As a reactive hydrocarbon species, the mixing ratios of toluene rapidly decreased
430 with height in daytime (defined as the period of 11:00-16:00 LT, as shown in Figure 7)
431 due to the combined effects of atmospheric dilution and OH-initiated chemical removal.
432 By contrast, the mixing ratios of ozone and formic acid increased with height. The

433 mixing ratios of ozone and formic acid all rapidly increased with height below 102 m,
434 predominantly attributed to the reduced effect of surface dry deposition with the
435 increase in height. The mean mixing ratios of formic acid increased by 18% from 102
436 m to 320 m in daytime, while ozone mixing ratios were well mixed above 102 m. Our
437 results point to the likely importance of photochemistry as a source of formic acid that
438 is enhanced with increasing height within the boundary layer.

439 The precursors and formation mechanisms of atmospheric formic acid have been
440 extensively investigated in previous studies but still remain uncertain. Isoprene has long
441 been recognized as an important precursor of formic acid through reactions with O₃ and
442 OH radicals (*Neeb et al., 1997; Paulot et al., 2009*). Recent studies also found that the
443 degradation of organic aerosols (OA) derived from isoprene is an important source of
444 formic acid (*Cope et al., 2021; Bates et al., 2023*). In addition, the photooxidation of
445 other biogenic and anthropogenic hydrocarbons is also a key source of formic acid
446 (*Paulot et al., 2011; Millet et al., 2015; Link et al., 2021*). Figure 9 illustrates the mean
447 vertical profiles of several key precursors of formic acid in daytime. The concentrations
448 of isoprene and toluene (Figure 7) all decreased rapidly with height. By contrast, MVK
449 and MACR, the primary oxidation products of isoprene (*Grosjean et al., 1993*),
450 exhibited weak vertical gradients. Formaldehyde, a more general photooxidation
451 product of VOCs, exhibited similar vertical distribution patterns to those of ozone.
452 Large amounts of OVOCs were produced and accumulated in higher altitudes through
453 the oxidation of hydrocarbons and the further oxidation of some OVOCs during their
454 upward mixing course. MVK, MACR, and formaldehyde are also key precursors of
455 formic acid. MVK and MACR can react with O₃ to produce formic acid (*Link et al.,*
456 *2020*). Formaldehyde can be converted to methanediol in cloud droplets and then be
457 rapidly oxidized by OH to produce formic acid (*Franco et al., 2021*). In addition, enol
458 (*Lei et al., 2020*) and many other OVOCs (such as glycolaldehyde (*Butkovskaya et al.,*
459 *2006a*) and hydroxyacetone (*Butkovskaya et al., 2006b*) can be further oxidized to
460 produce formic acid. Therefore, high concentrations of OVOCs aloft may be the

461 dominant factor that largely enhances the photochemical formation of formic acid in
462 urban regions.

463 As discussed above, formic acid exhibited strong positive vertical gradients
464 throughout the day, implying that the concentrations of formic acid measured at ground
465 level were not capable of accurately characterizing its abundance and temporal
466 variability in the whole boundary layer. Besides, the formic acid formed in daytime and
467 retained in the nocturnal residual layer also has vital impacts on the budget of formic
468 acid in the boundary layer. Thus, we used the column-integrated concentration (CIC)
469 of formic acid (the sum of the abundance in both the nocturnal residual layer and the
470 boundary layer, see detailed definitions in SI) to further clarify the diurnal variability
471 in the abundance of formic acid in the boundary layer.

472 As shown in Figure 10, the CICs of formic acid had a flatter diurnal pattern in
473 comparison to those at ground level. The CICs of formic acid had approximately stable
474 values overnight and reached a maximum at 16:00 LT. The ratio of the maximum and
475 minimum of CIC for formic acid was only 1.3, while it was 4.2 for the concentrations
476 of formic acid at 5 m. These results imply that the removal of atmospheric formic acid
477 (e.g., surface deposition and various chemical reactions) may be highly overestimated
478 if only ground-level measurements were used or constrained in numerical models. The
479 budget of the formic acid in high altitudes in the boundary layer was distinctly different
480 from those near the surface. As the result, numerical models cannot accurately
481 reproduce the abundances and budgets of formic acid without the constraints of vertical
482 observations and the clarification of formic acid formation mechanisms.

483 **3.3. Vertical variations and sources of isocyanic acid**

484 The mixing ratios of isocyanic acid also exhibited strong temporal variations
485 during the campaign with a mean of 0.28 ± 0.16 ppbv at 5 m and a mean of 0.43 ± 0.21
486 ppbv at 320 m, as shown in Figure 11. The mixing ratios of isocyanic acid measured at
487 the ground level in urban Beijing were approximately 10 times higher than those
488 measured in Los Angeles, USA (0.025 ppbv) (Roberts *et al.*, 2014) and Calgary, Canada

489 (0.036 ppbv) (*Woodward-Massey et al., 2014*) but were lower than those measured in
490 other regions in China. For example, the mean mixing ratio of isocyanic acid was 0.37
491 ppbv at a rural site (Gucheng) in the North China Plain (NCP), and 0.46 ppbv in urban
492 Guangzhou in the Pearl River Delta (PRD) region (*Wang et al., 2020*). Isocyanic acid
493 will pose a threat to human health when its ambient mixing ratios exceed 1.0 ppbv. In
494 this study, isocyanic acid mixing ratios greater than 1.0 ppbv were not observed at
495 ground level but were observed at 320 m on three days. The maximum hourly mixing
496 ratios of isocyanic acid at 320 m reached 1.63 ppbv at 16:00 LT on July 8th.

497 The mixing ratios of isocyanic acid at the five altitudes exhibited similar diurnal
498 variation patterns. After sunrise, the mixing ratios of isocyanic acid at the five altitudes
499 all simultaneously increased and peaked at about 14:00 LT. Then, isocyanic acid mixing
500 ratios decreased slowly and reached the minimum before sunrise the following day.
501 This diurnal variation pattern of isocyanic acid measured at the ground level in urban
502 Beijing was not consistent with those measured at the Gucheng site in NCP (*Wang et*
503 *al., 2020*). The isocyanic acid mixing ratios at the Gucheng site exhibited insignificant
504 diurnal variability throughout the day with only a weak morning peak, predominantly
505 attributed to the enhancement of primary emissions. However, the diurnal variation
506 patterns of isocyanic acid measured at the five altitudes were well correlated with the
507 change in solar irradiance and were consistent with those measured at the two sites in
508 PRD. These results imply that ambient concentrations of isocyanic acid in urban Beijing
509 were mainly contributed by secondary sources associated with photochemical reactions.

510 Similar to formic acid, the simultaneous increase of isocyanic acid mixing ratios
511 at the five altitudes with the onset of sunlight also indicates the presence of adequate
512 precursors even in the nocturnal residual layer. In addition, the diurnal variability of
513 isocyanic acid mixing ratios measured below 200 m was much weaker than those
514 measured at 320 m. For example, the ratio of the daily maximum to the daily minimum
515 mixing ratios of isocyanic acid was 1.9 at 320 m, while the ratio was only 1.4 at 5 m.
516 The mean enhancement rate of isocyanic acid mixing ratios at 320 m (0.05 ppbv h^{-1})

517 between 6:00 and 10:00 LT was approximately five times larger than that at 5 m (0.01
518 ppbv h⁻¹). The vertical gradients of isocyanic acid between 102 and 320 m were also
519 larger than those below (Figure 12). The rapid increase in both concentrations and
520 enhancement rates of isocyanic acid with height (Figures 8 and 12) implies the
521 enhanced photochemical formation of isocyanic acid in the middle and upper part of
522 the boundary layer.

523 Secondary formation precursors of atmospheric isocyanic acid were still poorly
524 understood so far. Amides were considered important precursors of isocyanic acid
525 (*Roberts et al., 2014; Rosanka et al., 2020*). As reported in our previous study (*Wang*
526 *et al., 2020*), C₃ amides accounted for the largest fraction of the total concentrations of
527 amides and were dominant contributors to the secondary formation of isocyanic acid.
528 The mixing ratios of C₃ amides in Guangzhou in PRD exhibited strong diurnal
529 variations. Along with the sunrise, the mixing ratios of C₃ amides rapidly decreased and
530 reached the minimum at 13:00 LT. Afterward, the mixing ratios of C₃ amides started to
531 increase and accumulated at night. As shown in Figure S4, the influence of long tubing
532 on the measurement of amides was limited, so we also measured the amides during the
533 field campaign. However, the mixing ratios of C₃ amides in Beijing and Gucheng in
534 NCP exhibited insignificant diurnal variability, consistent with those of isocyanic acid.
535 The mean mixing ratios of C₃ amides at 5 m in urban Beijing is only 0.03 ppbv during
536 the campaign, which is one order of magnitude lower than those in Guangzhou (0.35
537 ppbv) and Gucheng (0.18 ppbv). The mixing ratios of C₃ amides measured at the five
538 altitudes in urban Beijing were also approximately one order of magnitude lower than
539 those of isocyanic acid (Figure 12). Besides, the mixing ratios of C₃ amides decreased
540 with height in both nighttime and daytime, indicating predominant contributions from
541 primary emissions. This is consistent with the fact that primary emissions of chemical
542 composition from industry-related sources have been largely reduced with the outward
543 migration of industry in urban Beijing. By contrast, the mixing ratios of isocyanic acid
544 increased with height in both day and night with an average of 0.32 ppbv at 5 m and

545 0.60 ppbv at 320 m. These results suggest that C₃ amides were far more enough to
546 account for the secondary formation of isocyanic acid in urban Beijing.

547 Figure 13(a) gives the composition and average concentrations of C₁-C₁₀ amides
548 measured at the five altitudes during the campaign. C₂ amides accounted for the largest
549 fraction of the total mixing ratios of amides. The total mixing ratios of amides exhibited
550 decreasing tendencies with the increase in height, suggesting predominant contributions
551 from direct emissions of surface sources. As for formamide, its mixing ratios exhibited
552 an increasing tendency from 0.024 ppbv at 5 m to 0.030 ppbv at 320 m. The positive
553 vertical gradients of formamide suggest its enhanced formation with height, probably
554 due to the enhancements of formic acid. However, the average concentration ratios of
555 formamide to formic acid slightly varied between 0.01 and 0.02 among the five heights.
556 The average concentration ratios of formamide to isocyanic acid decreased from 0.09
557 at 5 m to 0.07 at 320 m. These results imply that the formation of isocyanic acid through
558 the pathway of HCOOH-CH₃NO-HNCO may be enhanced with the increase in height
559 but could only contribute a tiny fraction of the observed isocyanic acid, as shown in
560 Figure 13(b). Assuming the full conversion of C₁-C₁₀ amides to isocyanic acid, the
561 average concentration ratios of amides (sum of C₁-C₁₀) to isocyanic acid below 320 m
562 only ranged between 0.32 and 0.56 and decreased with height. Therefore, in addition to
563 amides, there must be other important precursors and formation pathways of isocyanic
564 acid, particularly in high altitudes. The simultaneous increase of isocyanic acid
565 concentrations at the five heights upon sunrise (Figure 11) implies the presence of
566 adequate precursors in the nocturnal residual layer. The oxidation products of VOCs
567 driven by ozone and NO₃ radicals in nighttime may be an important class of precursors.
568 In addition, the largest enhancement rates and highest concentrations of isocyanic acid
569 at 320 m in daytime also suggest that high concentrations of OVOCs and low-NO_x
570 conditions may enhance the secondary formation of isocyanic acid.

571 The positive vertical gradients of isocyanic acid imply that the secondary
572 formation of isocyanic acid aloft could serve as an important source of surface isocyanic

573 acid in daytime driven by turbulence mixing. The CICs of isocyanic acid were
574 calculated to further clarify its abundance and temporal variability in the whole
575 boundary layer. Distinct diurnal patterns were observed between the ground-level
576 concentrations and CICs of isocyanic acid. Analogous to formic acid, the CICs of
577 isocyanic acid varied insignificantly over nighttime and enhanced in daytime, reaching
578 the maximum at approximately 14:00 LT. The formation of some chemicals can be
579 largely enhanced at higher altitudes and so using ground-level measurements to
580 constrain numerical models may be not adequate.

581 **4. Conclusion**

582 In this study, vertical and diurnal variations of formic and isocyanic acids in
583 urban Beijing were investigated using tower-based online gradient measurements. The
584 measurements of isocyanic acid can be well measured through long PFA Teflon tubes.
585 The measurements of formic acid made through long tubes were slightly influenced by
586 the memory effect of tubing walls, and the vertical increasing gradients of formic acid
587 may be slightly enhanced if the tubing effects were considered. The concentrations of
588 formic and isocyanic acids all increased with height in both nighttime and daytime. The
589 diurnal and vertical distribution patterns of formic and isocyanic acids all suggest that
590 their abundances in the boundary layer were dominantly contributed by secondary
591 formation associated with photochemical reactions. The photochemical formations of
592 formic and isocyanic acids were also substantially enhanced with the increase in height.
593 The formation pathway of isocyanic acid through $\text{HCOOH-CH}_3\text{NO-HNCO}$ only
594 accounted for a tiny fraction of its ambient abundance. The formic and isocyanic acids
595 photochemically formed in the middle and upper parts of the boundary layer were
596 important sources for those at ground level in urban region. The differences of the
597 diurnal patterns between CICs and ground-level concentrations of formic and isocyanic
598 acids further highlight the importance of vertical observations in elucidating their
599 budgets and sources in the whole boundary layer.

600 Characterization of the vertical variations in formic and isocyanic acids could
601 provide valuable information for elucidating their budgets and sources in the boundary
602 layer. However, there are still many important but unresolved questions associated with
603 the vertical distributions of formic and isocyanic acids. For example, the key precursors
604 that drive the rapid formation of formic and isocyanic acids in the residual layer are still
605 unknown. Are there any changes in the key precursors and formation pathways of
606 formic and isocyanic acids with the increase of height in urban region? To answer these
607 questions, the combination of vertical gradient measurements of more chemical species
608 and numerical simulations is needed in future studies.

609 **Supporting Information:** Additional experimental details, materials, and methods,
610 including schematic illustration of tubing test, determination of the long tubes'
611 cumulative influence, and calculation of CICs.

612 **Data availability**

613 Data related to this article are available online at
614 <https://doi.org/10.7910/DVN/ANH0WE>.

615 **Author contributions**

616 QY, XBL, BY, and YH designed the research. QY, XBL, BY, XZ, YH, LY, XH,
617 JQ and MS contributed to the data collection and data analysis. QY and XBL wrote the
618 paper with contributions from all coauthors. All the coauthors discussed the results and
619 reviewed the paper.

620 **Competing interests**

621 The authors declare that they have no conflict of interest.

622 **Acknowledgment**

623 This work was financially supported by the National Key R&D Plan of China
624 (grant No. 2023YFC3706103, 2023YFC3706201, 2022YFC3700604) and the National

625 Natural Science Foundation of China (grant No. 42121004, 42275103, 42205904,
626 42230701, 42305095). This work was also supported by the Special Fund Project for
627 Science and Technology Innovation Strategy of Guangdong Province (Grant No.
628 2019B121205004). The authors would like to thank the personnel who participated in
629 data collection, instrument maintenance, and logistic support during the field campaign.

630 **Reference**

- 631 Acton, W. J. F., Huang, Z., Davison, B., Drysdale, W. S., Fu, P., Hollaway, M., Langford,
632 B., Lee, J., Liu, Y., Metzger, S., Mullinger, N., Nemitz, E., Reeves, C. E., Squires, F.
633 A., Vaughan, A. R., Wang, X., Wang, Z., Wild, O., Zhang, Q., Zhang, Y., and Hewitt,
634 C. N.: Surface–atmosphere fluxes of volatile organic compounds in Beijing,
635 *Atmospheric Chemistry and Physics*, 20, 15101-15125, 10.5194/acp-20-15101-2020,
636 2020.
- 637 Alwe, H. D., Millet, D. B., Chen, X., Raff, J. D., Payne, Z. C., and Fledderman, K.:
638 Oxidation of Volatile Organic Compounds as the Major Source of Formic Acid in a
639 Mixed Forest Canopy, *Geophysical Research Letters*, 46, 2940-2948,
640 <https://doi.org/10.1029/2018GL081526>, 2019.
- 641 Andreae, M. O., Talbot, R. W., Andreae, T. W., and Harriss, R. C.: Formic and acetic
642 acid over the central Amazon region, Brazil: 1. Dry season, *Journal of Geophysical*
643 *Research: Atmospheres*, 93, 1616-1624, <https://doi.org/10.1029/JD093iD02p01616>,
644 1988.
- 645 Bannan, T. J., Bacak, A., Muller, J. B. A., Booth, A. M., Jones, B., Le Breton, M.,
646 Leather, K. E., Ghalaieny, M., Xiao, P., Shallcross, D. E., and Percival, C. J.:
647 Importance of direct anthropogenic emissions of formic acid measured by a chemical
648 ionisation mass spectrometer (CIMS) during the Winter ClearfLo Campaign in
649 London, January 2012, *Atmospheric Environment*, 83, 301-310,
650 10.1016/j.atmosenv.2013.10.029, 2014.
- 651 Bannan, T. J., Murray Booth, A., Le Breton, M., Bacak, A., Muller, J. B. A., Leather, K.
652 E., Khan, M. A. H., Lee, J. D., Dunmore, R. E., Hopkins, J. R., Fleming, Z. L., Sheps,
653 L., Taatjes, C. A., Shallcross, D. E., and Percival, C. J.: Seasonality of Formic Acid
654 (HCOOH) in London during the ClearfLo Campaign, *Journal of Geophysical*
655 *Research: Atmospheres*, 122, 10.1002/2017jd027064, 2017.
- 656 Barnes, I., Solignac, G., Mellouki, A., and Becker, K. H.: Aspects of the atmospheric
657 chemistry of amides, *ChemPhyChem*, 11, 3844-3857, 10.1002/cphc.201000374,
658 2010.
- 659 Bates, K. H., Jacob, D. J., Cope, J. D., Chen, X., Millet, D. B., and Nguyen, T. B.:
660 Emerging investigator series: aqueous oxidation of isoprene-derived organic aerosol
661 species as a source of atmospheric formic and acetic acids, *Environmental Science:*
662 *Atmospheres*, 10.1039/d3ea00076a, 2023.

663 Benish, S. E., He, H., Ren, X., Roberts, S. J., Salawitch, R. J., Li, Z., Wang, F., Wang,
664 Y., Zhang, F., Shao, M., Lu, S., and Dickerson, R. R.: Measurement report: Aircraft
665 observations of ozone, nitrogen oxides, and volatile organic compounds over Hebei
666 Province, China, *Atmospheric Chemistry and Physics*, 20, 14523-14545,
667 10.5194/acp-20-14523-2020, 2020.

668 Borduas, N., Murphy, J. G., Wang, C., Silva, G. d., Abbatt, J. P. D. J. E. S., and Letters,
669 T.: Gas Phase Oxidation of Nicotine by OH Radicals: Kinetics, Mechanisms, and
670 Formation of HNCO, 3, 327-331, 2016.

671 Butkovskaya, N. I., Pouvesle, N., Kukui, A., and Le Bras, G.: Mechanism of the OH-
672 Initiated Oxidation of Glycolaldehyde over the Temperature Range 233–296 K, *The*
673 *Journal of Physical Chemistry A*, 110, 13492-13499, 10.1021/jp064993k, 2006a.

674 Butkovskaya, N. I., Pouvesle, N., Kukui, A., Mu, Y., and Le Bras, G.: Mechanism of
675 the OH-Initiated Oxidation of Hydroxyacetone over the Temperature Range 236–298
676 K, *The Journal of Physical Chemistry A*, 110, 6833-6843, 10.1021/jp056345r, 2006b.

677 Chandra, B. P. and Sinha, V.: Contribution of post-harvest agricultural paddy residue
678 fires in the N.W. Indo-Gangetic Plain to ambient carcinogenic benzenoids, toxic
679 isocyanic acid and carbon monoxide, *Environment International*, 88, 187-197,
680 10.1016/j.envint.2015.12.025, 2016.

681 Chebbi, A. and Carlier, P.: Carboxylic acids in the troposphere, occurrence, sources,
682 and sinks: A review, *Atmospheric Environment*, 30, 4233-4249,
683 [https://doi.org/10.1016/1352-2310\(96\)00102-1](https://doi.org/10.1016/1352-2310(96)00102-1), 1996.

684 Cope, J. D., Abellar, K. A., Bates, K. H., Fu, X., and Nguyen, T. B.: Aqueous
685 Photochemistry of 2-Methyltetrol and Erythritol as Sources of Formic Acid and
686 Acetic Acid in the Atmosphere, *ACS Earth and Space Chemistry*, 5, 1265-1277,
687 10.1021/acsearthspacechem.1c00107, 2021.

688 De Gouw, J. A., Gilman, J. B., Kim, S. W., Alvarez, S. L., Dusanter, S., Graus, M.,
689 Griffith, S. M., Isaacman - VanWertz, G., Kuster, W. C., Lefer, B. L., Lerner, B. M.,
690 McDonald, B. C., Rappenglück, B., Roberts, J. M., Stevens, P. S., Stutz, J., Thalman,
691 R., Veres, P. R., Volkamer, R., Warneke, C., Washenfelder, R. A., and Young, C. J.:
692 Chemistry of Volatile Organic Compounds in the Los Angeles Basin: Formation of
693 Oxygenated Compounds and Determination of Emission Ratios, *Journal of*
694 *Geophysical Research: Atmospheres*, 123, 2298-2319, 10.1002/2017jd027976, 2018.

695 Deming, B. L., Pagonis, D., Liu, X., Day, D. A., Talukdar, R., Krechmer, J. E., de Gouw,
696 J. A., Jimenez, J. L., and Ziemann, P. J.: Measurements of delays of gas-phase
697 compounds in a wide variety of tubing materials due to gas-wall interactions,
698 *Atmospheric Measurement Techniques*, 12, 3453-3461, 10.5194/amt-12-3453-2019,
699 2019.

700 Enders, G., Dlugi, R., Steinbrecher, R., Clement, B., Daiber, R., Eijk, J. v., Gäb, S.,
701 Haziza, M., Helas, G., Herrmann, U., Kessel, M., Kesselmeier, J., Kotzias, D.,
702 Kourtidis, K., Kurth, H. H., McMillen, R. T., Roeder, G., Schürmann, W., Teichmann,
703 U., and Torres, L.: Biosphere/Atmosphere interactions: Integrated research in a
704 European coniferous forest ecosystem, *Atmospheric Environment*, 26, 171-189,

705 [https://doi.org/10.1016/0960-1686\(92\)90269-Q](https://doi.org/10.1016/0960-1686(92)90269-Q), 1992.

706 Fang, X., Shao, M., Stohl, A., Zhang, Q., Zheng, J., Guo, H., Wang, C., Wang, M., Ou,
707 J., Thompson, R. L., and Prinn, R. G.: Top-down estimates of benzene and toluene
708 emissions in the Pearl River Delta and Hong Kong, China, *Atmospheric Chemistry
709 and Physics*, 16, 3369-3382, 10.5194/acp-16-3369-2016, 2016.

710 Franco, B., Blumenstock, T., Cho, C., Clarisse, L., Clerbaux, C., Coheur, P. F., De
711 Mazière, M., De Smedt, I., Dorn, H. P., Emmerichs, T., Fuchs, H., Gkatzelis, G.,
712 Griffith, D. W. T., Gromov, S., Hannigan, J. W., Hase, F., Hohaus, T., Jones, N.,
713 Kerkweg, A., Kiendler-Scharr, A., Lutsch, E., Mahieu, E., Novelli, A., Ortega, I.,
714 Paton-Walsh, C., Pommier, M., Pozzer, A., Reimer, D., Rosanka, S., Sander, R.,
715 Schneider, M., Strong, K., Tillmann, R., Van Roozendael, M., Vereecken, L.,
716 Vigouroux, C., Wahner, A., and Taraborrelli, D.: Ubiquitous atmospheric production
717 of organic acids mediated by cloud droplets, *Nature*, 593, 233-237, 10.1038/s41586-
718 021-03462-x, 2021.

719 Fulgham, S. R., Brophy, P., Link, M., Ortega, J., Pollack, I., and Farmer, D. K.: Seasonal
720 Flux Measurements over a Colorado Pine Forest Demonstrate a Persistent Source of
721 Organic Acids, *ACS Earth and Space Chemistry*, 3, 2017-2032,
722 10.1021/acsearthspacechem.9b00182, 2019.

723 Galloway, J. N., Likens, G. E., Keene, W. C., and Miller, J. M.: The composition of
724 precipitation in remote areas of the world, *Journal of Geophysical Research: Oceans*,
725 87, 8771-8786, <https://doi.org/10.1029/JC087iC11p08771>, 1982.

726 Goode, J. G., Yokelson, R. J., Ward, D. E., Susott, R. A., Babbitt, R. E., Davies, M. A.,
727 and Hao, W. M.: Measurements of excess O₃, CO₂, CO, CH₄, C₂H₄, C₂H₂, HCN,
728 NO, NH₃, HCOOH, CH₃COOH, HCHO, and CH₃OH in 1997 Alaskan biomass
729 burning plumes by airborne Fourier transform infrared spectroscopy (AFTIR),
730 *Journal of Geophysical Research: Atmospheres*, 105, 22147-22166,
731 10.1029/2000jd900287, 2000.

732 Grosjean, D., Williams, E. L., II, and Grosjean, E.: Atmospheric chemistry of isoprene
733 and of its carbonyl products, *Environmental Science & Technology*, 27, 830-840,
734 10.1021/es00042a004, 1993.

735 Helmig, D., Johnson, B., Oltmans, S., Neff, W., Eisele, F., and Davis, D.: Elevated
736 ozone in the boundary layer at South Pole, *Atmospheric Environment*, 42, 2788-2803,
737 10.1016/j.atmosenv.2006.12.032, 2008a.

738 Helmig, D., Johnson, B., Warshawsky, M., Morse, T., Neff, W., Eisele, F., and Davis,
739 D.: Nitric oxide in the boundary-layer at South Pole during the Antarctic
740 Tropospheric Chemistry Investigation (ANTCI), *Atmospheric Environment*, 42,
741 2817-2830, 10.1016/j.atmosenv.2007.03.061, 2008b.

742 Hems, R. F., Wang, C., Collins, D. B., Zhou, S., Borduas-Dedekind, N., Siegel, J. A.,
743 and Abbatt, J. P. D.: Sources of isocyanic acid (HNCO) indoors: a focus on cigarette
744 smoke, *Environmental Science: Processes & Impacts*, 21, 1334-1341,
745 10.1039/c9em00107g, 2019.

746 Hu, L., Millet, D. B., Kim, S. Y., Wells, K. C., Griffis, T. J., Fischer, E. V., Helmig, D.,

747 Hueber, J., and Curtis, A. J.: North American acetone sources determined from tall
748 tower measurements and inverse modeling, *Atmospheric Chemistry and Physics*, 13,
749 3379-3392, 10.5194/acp-13-3379-2013, 2013.

750 Hu, X., Yang, G., Liu, Y., Lu, Y., Wang, Y., Chen, H., Chen, J., and Wang, L.:
751 Atmospheric gaseous organic acids in winter in a rural site of the North China Plain,
752 *Journal of Environmental Sciences*, 113, 190-203, 10.1016/j.jes.2021.05.035, 2022.

753 Jacob, D. J.: Chemistry of OH in remote clouds and its role in the production of formic
754 acid and peroxymonosulfate, *Journal of Geophysical Research: Atmospheres*, 91,
755 9807-9826, <https://doi.org/10.1029/JD091iD09p09807>, 1986.

756 Jaisson, S., Pietrement, C., and Gillery, P.: Carbamylation-derived products: bioactive
757 compounds and potential biomarkers in chronic renal failure and atherosclerosis,
758 *Clinical chemistry*, 57, 1499-1505, 10.1373/clinchem.2011.163188, 2011.

759 Jathar, S. H., Heppding, C., Link, M. F., Farmer, D. K., Akherati, A., Kleeman, M. J.,
760 de Gouw, J. A., Veres, P. R., and Roberts, J. M.: Investigating diesel engines as an
761 atmospheric source of isocyanic acid in urban areas, *Atmospheric Chemistry and
762 Physics*, 17, 8959-8970, 10.5194/acp-17-8959-2017, 2017.

763 Ji, Y., Huey, L. G., Tanner, D. J., Lee, Y. R., Veres, P. R., Neuman, J. A., Wang, Y., and
764 Wang, X.: A vacuum ultraviolet ion source (VUV-IS) for iodide-chemical ionization
765 mass spectrometry: a substitute for radioactive ion sources, *Atmospheric
766 Measurement Techniques*, 13, 3683-3696, 10.5194/amt-13-3683-2020, 2020.

767 Karion, A., Sweeney, C., Tans, P., and Newberger, T.: AirCore: An Innovative
768 Atmospheric Sampling System, *Journal of Atmospheric and Oceanic Technology*, 27,
769 1839-1853, 10.1175/2010jtecha1448.1, 2010.

770 Kawamura, K. and Kaplan, I. R.: Organic compounds in the rainwater of Los Angeles,
771 *Environmental Science & Technology*, 17, 497-501, 10.1021/es00114a011, 1983.

772 Kawamura, K., Steinberg, S., and Kaplan, I. R.: Homologous series of C1-C10
773 monocarboxylic acids and C1-C6 carbonyls in Los Angeles air and motor vehicle
774 exhausts, *Atmospheric Environment*, 34, 4175-4191, [https://doi.org/10.1016/S1352-
775 2310\(00\)00212-0](https://doi.org/10.1016/S1352-2310(00)00212-0), 2000.

776 Keene, W. C. and Galloway, J. N.: Organic acidity in precipitation of North America,
777 *Atmospheric Environment*, 18, 2491-2497, [https://doi.org/10.1016/0004-
778 6981\(84\)90020-9](https://doi.org/10.1016/0004-6981(84)90020-9), 1984.

779 Kesselmeier, J., Bode, K., Gerlach, C., and Jork, E. M.: Exchange of atmospheric
780 formic and acetic acids with trees and crop plants under controlled chamber and
781 purified air conditions, *Atmospheric Environment*, 32, 1765-1775,
782 [https://doi.org/10.1016/S1352-2310\(97\)00465-2](https://doi.org/10.1016/S1352-2310(97)00465-2), 1998.

783 Khare, P., Kumar, N., Kumari, K. M., and Srivastava, S. S.: Atmospheric formic and
784 acetic acids: An overview, *Reviews of Geophysics*, 37, 227-248,
785 <https://doi.org/10.1029/1998RG900005>, 1999.

786 Koeth, R. A., Kalantar-Zadeh, K., Wang, Z., Fu, X., Tang, W. H., and Hazen, S. L.:
787 Protein carbamylation predicts mortality in ESRD, *Journal of the American Society
788 of Nephrology*, 24, 853-861, 10.1681/ASN.2012030254, 2013.

789 Krechmer, J. E., Day, D. A., Ziemann, P. J., and Jimenez, J. L.: Direct Measurements
790 of Gas/Particle Partitioning and Mass Accommodation Coefficients in
791 Environmental Chambers, *Environmental science & technology*, 51, 11867-11875,
792 10.1021/acs.est.7b02144, 2017.

793 Le Breton, M., Bacak, A., Muller, J. B. A., Xiao, P., Shallcross, B. M. A., Batt, R.,
794 Cooke, M. C., Shallcross, D. E., Bauguitte, S. J. B., and Percival, C. J.: Simultaneous
795 airborne nitric acid and formic acid measurements using a chemical ionization mass
796 spectrometer around the UK: Analysis of primary and secondary production
797 pathways, *Atmospheric Environment*, 83, 166-175, 10.1016/j.atmosenv.2013.10.008,
798 2014.

799 Lei, X., Wang, W., Gao, J., Wang, S., and Wang, W.: Atmospheric Chemistry of Enols:
800 The Formation Mechanisms of Formic and Peroxyformic Acids in Ozonolysis of
801 Vinyl Alcohol, *The Journal of Physical Chemistry A*, 124, 4271-4279,
802 10.1021/acs.jpca.0c01480, 2020.

803 Li, T., Wang, Z., Yuan, B., Ye, C., Lin, Y., Wang, S., Sha, Q. e., Yuan, Z., Zheng, J., and
804 Shao, M.: Emissions of carboxylic acids, hydrogen cyanide (HCN) and isocyanic
805 acid (HNCO) from vehicle exhaust, *Atmospheric Environment*, 247,
806 10.1016/j.atmosenv.2021.118218, 2021.

807 Li, X.-B., Yuan, B., Wang, S., Wang, C., Lan, J., Liu, Z., Song, Y., He, X., Huangfu, Y.,
808 Pei, C., Cheng, P., Yang, S., Qi, J., Wu, C., Huang, S., You, Y., Chang, M., Zheng, H.,
809 Yang, W., Wang, X., and Shao, M.: Variations and sources of volatile organic
810 compounds (VOCs) in urban region: insights from measurements on a tall tower,
811 *Atmospheric Chemistry and Physics*, 22, 10567-10587, 10.5194/acp-22-10567-2022,
812 2022.

813 Li, X., Zhang, C., Liu, A., Yuan, B., Yang, H., Liu, C., Wang, S., Huangfu, Y., Qi, J.,
814 Liu, Z., He, X., Song, X., Chen, Y., Peng, Y., Zhang, X., Zheng, E., Yang, L., Yang,
815 Q., Qin, G., Zhou, J., and Shao, M.: Assessment of Long Tubing in Measuring
816 Atmospheric Trace Gases: Applications on Tall Towers, *Environmental Science:
817 Atmospheres*, 506-520, 10.1039/d2ea00110a, 2023.

818 Liggio, J., Moussa, S. G., Wentzell, J., Darlington, A., Liu, P., Leithead, A., Hayden, K.,
819 O'Brien, J., Mittermeier, R. L., Staebler, R., Wolde, M., and Li, S.-M.: Understanding
820 the primary emissions and secondary formation of gaseous organic acids in the oil
821 sands region of Alberta, Canada, *Atmospheric Chemistry and Physics*, 17, 8411-8427,
822 10.5194/acp-17-8411-2017, 2017.

823 Link, M. F., Brophy, P., Fulgham, S. R., Murschell, T., and Farmer, D. K.: Isoprene
824 versus Monoterpenes as Gas-Phase Organic Acid Precursors in the Atmosphere, *ACS
825 Earth and Space Chemistry*, 5, 1600-1612, 10.1021/acsearthspacechem.1c00093,
826 2021.

827 Link, M. F., Nguyen, T. B., Bates, K., Müller, J.-F., and Farmer, D. K.: Can Isoprene
828 Oxidation Explain High Concentrations of Atmospheric Formic and Acetic Acid over
829 Forests?, *ACS Earth and Space Chemistry*, 4, 730-740,
830 10.1021/acsearthspacechem.0c00010, 2020.

831 Liu, X., Deming, B., Pagonis, D., Day, D. A., Palm, B. B., Talukdar, R., Roberts, J. M.,
832 Veres, P. R., Krechmer, J. E., Thornton, J. A., de Gouw, J. A., Ziemann, P. J., and
833 Jimenez, J. L.: Effects of gas–wall interactions on measurements of semivolatile
834 compounds and small polar molecules, *Atmospheric Measurement Techniques*, 12,
835 3137-3149, 10.5194/amt-12-3137-2019, 2019.

836 Lopez-Hilfiker, F. D., Mohr, C., Ehn, M., Rubach, F., Kleist, E., Wildt, J., Mentel, T. F.,
837 Lutz, A., Hallquist, M., Worsnop, D., and Thornton, J. A.: A novel method for online
838 analysis of gas and particle composition: description and evaluation of a Filter Inlet
839 for Gases and AEROSols (FIGAERO), *Atmospheric Measurement Techniques*, 7,
840 983-1001, 10.5194/amt-7-983-2014, 2014.

841 Mattila, J. M., Brophy, P., Kirkland, J., Hall, S., Ullmann, K., Fischer, E. V., Brown, S.,
842 McDuffie, E., Tevlin, A., and Farmer, D. K.: Tropospheric sources and sinks of gas-
843 phase acids in the Colorado Front Range, *Atmospheric Chemistry and Physics*, 18,
844 12315-12327, 10.5194/acp-18-12315-2018, 2018.

845 Meng, F., Qin, M., Tang, K., Duan, J., Fang, W., Liang, S., Ye, K., Xie, P., Sun, Y., Xie,
846 C., Ye, C., Fu, P., Liu, J., and Liu, W.: High-resolution vertical distribution and
847 sources of HONO and NO₂ in the nocturnal boundary layer
848 in urban Beijing, China, *Atmospheric Chemistry and Physics*, 20, 5071-5092,
849 10.5194/acp-20-5071-2020, 2020.

850 Millet, D. B., Baasandorj, M., Farmer, D. K., Thornton, J. A., Baumann, K., Brophy, P.,
851 Chaliyakunnel, S., de Gouw, J. A., Graus, M., Hu, L., Koss, A., Lee, B. H., Lopez-
852 Hilfiker, F. D., Neuman, J. A., Paulot, F., Peischl, J., Pollack, I. B., Ryerson, T. B.,
853 Warneke, C., Williams, B. J., and Xu, J.: A large and ubiquitous source of
854 atmospheric formic acid, *Atmospheric Chemistry and Physics*, 15, 6283-6304,
855 10.5194/acp-15-6283-2015, 2015.

856 Mungall, E. L., Abbatt, J. P. D., Wentzell, J. J. B., Wentworth, G. R., Murphy, J. G.,
857 Kunkel, D., Gute, E., Tarasick, D. W., Sharma, S., Cox, C. J., Uttal, T., and Liggio,
858 J.: High gas-phase mixing ratios of formic and acetic acid in the High Arctic,
859 *Atmospheric Chemistry and Physics*, 18, 10237-10254, 10.5194/acp-18-10237-2018,
860 2018.

861 Mydel, P., Wang, Z., Brisslert, M., Hellvard, A., Dahlberg, L. E., Hazen, S. L., and
862 Bokarewa, M. I. J. T. J. o. I.: Carbamylation-Dependent Activation of T Cells: A
863 Novel Mechanism in the Pathogenesis of Autoimmune Arthritis, *The Journal of*
864 *Immunology*, 184, 6882 - 6890, 2010.

865 Neeb, P., Sauer, F., Horie, O., and Moortgat, G. K.: Formation of hydroxymethyl
866 hydroperoxide and formic acid in alkene ozonolysis in the presence of water vapour,
867 *Atmospheric Environment*, 31, 1417-1423, [https://doi.org/10.1016/S1352-
868 2310\(96\)00322-6](https://doi.org/10.1016/S1352-2310(96)00322-6), 1997.

869 Pagonis, D., Krechmer, J. E., de Gouw, J., Jimenez, J. L., and Ziemann, P. J.: Effects of
870 gas–wall partitioning in Teflon tubing and instrumentation on time-resolved
871 measurements of gas-phase organic compounds, *Atmospheric Measurement*
872 *Techniques*, 10, 4687-4696, 10.5194/amt-10-4687-2017, 2017.

873 Palm, B. B., Liu, X., Jimenez, J. L., and Thornton, J. A.: Performance of a new coaxial
874 ion–molecule reaction region for low-pressure chemical ionization mass
875 spectrometry with reduced instrument wall interactions, *Atmospheric Measurement*
876 *Techniques*, 12, 5829-5844, 10.5194/amt-12-5829-2019, 2019.

877 Paulot, F., Crouse, J. D., Kjaergaard, H. G., Kroll, J. H., Seinfeld, J. H., and Wennberg,
878 P. O.: Isoprene photooxidation: new insights into the production of acids and organic
879 nitrates, *Atmospheric Chemistry and Physics*, 9, 1479-1501, 10.5194/acp-9-1479-
880 2009, 2009.

881 Paulot, F., Wunch, D., Crouse, J. D., Toon, G. C., Millet, D. B., DeCarlo, P. F.,
882 Vigouroux, C., Deutscher, N. M., Gonzalez Abad, G., Notholt, J., Warneke, T.,
883 Hannigan, J. W., Warneke, C., de Gouw, J. A., Dunlea, E. J., De Maziere, M., Griffith,
884 D. W. T., Bernath, P., Jimenez, J. L., and Wennberg, P. O.: Importance of secondary
885 sources in the atmospheric budgets of formic and acetic acids, *Atmospheric*
886 *Chemistry and Physics*, 11, 1989-2013, 10.5194/acp-11-1989-2011, 2011.

887 Roberts, J. M. and Liu, Y.: Solubility and solution-phase chemistry of isocyanic acid,
888 methyl isocyanate, and cyanogen halides, *Atmospheric Chemistry and Physics*, 19,
889 4419-4437, 10.5194/acp-19-4419-2019, 2019.

890 Roberts, J. M., Veres, P. R., Cochran, A. K., Warneke, C., Burling, I. R., Yokelson, R.
891 J., Lerner, B., Gilman, J. B., Kuster, W. C., Fall, R., and de Gouw, J.: Isocyanic acid
892 in the atmosphere and its possible link to smoke-related health effects, *Proceedings*
893 *of the National Academy of Sciences*, 108, 8966-8971, 10.1073/pnas.1103352108,
894 2011.

895 Roberts, J. M., Veres, P. R., VandenBoer, T. C., Warneke, C., Graus, M., Williams, E.
896 J., Lefer, B., Brock, C. A., Bahreini, R., Öztürk, F., Middlebrook, A. M., Wagner, N.
897 L., Dubé, W. P., and de Gouw, J. A.: New insights into atmospheric sources and sinks
898 of isocyanic acid, HNCO, from recent urban and regional observations, *Journal of*
899 *Geophysical Research: Atmospheres*, 119, 1060-1072, 10.1002/2013jd019931, 2014.

900 Rosanka, S., Vu, G. H. T., Nguyen, H. M. T., Pham, T. V., Javed, U., Taraborrelli, D.,
901 and Vereecken, L.: Atmospheric chemical loss processes of isocyanic acid (HNCO):
902 a combined theoretical kinetic and global modelling study, *Atmospheric Chemistry*
903 *and Physics*, 20, 6671-6686, 10.5194/acp-20-6671-2020, 2020.

904 Schnitzhofer, R., Wisthaler, A., and Hansel, A.: Real-time profiling of organic trace
905 gases in the planetary boundary layer by PTR-MS using a tethered balloon,
906 *Atmospheric Measurement Techniques*, 2, 773-777, 10.5194/amt-2-773-2009, 2009.

907 Schobesberger, S., Lopez - Hilfiker, F. D., Taipale, D., Millet, D. B., D'Ambro, E. L.,
908 Rantala, P., Mammarella, I., Zhou, P., Wolfe, G. M., Lee, B. H., Boy, M., and
909 Thornton, J. A.: High upward fluxes of formic acid from a boreal forest canopy,
910 *Geophysical Research Letters*, 43, 9342-9351, 10.1002/2016gl069599, 2016.

911 Skorokhod, A. I., Berezina, E. V., Moiseenko, K. B., Elansky, N. F., and Belikov, I. B.:
912 Benzene and toluene in the surface air of northern Eurasia from TROICA-12
913 campaign along the Trans-Siberian Railway, *Atmospheric Chemistry and Physics*, 17,
914 5501-5514, 10.5194/acp-17-5501-2017, 2017.

915 Stavrakou, T., Müller, J. F., Peeters, J., Razavi, A., Clarisse, L., Clerbaux, C., Coheur,
916 P. F., Hurtmans, D., De Mazière, M., Vigouroux, C., Deutscher, N. M., Griffith, D.
917 W. T., Jones, N., and Paton-Walsh, C.: Satellite evidence for a large source of formic
918 acid from boreal and tropical forests, *Nature Geoscience*, 5, 26-30,
919 10.1038/ngeo1354, 2011.

920 Tan, Q., Ge, B., Xu, X., Gan, L., Yang, W., Chen, X., Pan, X., Wang, W., Li, J., and
921 Wang, Z.: Increasing impacts of the relative contributions of regional transport on air
922 pollution in Beijing: Observational evidence, *Environmental Pollution*, 292, 118407,
923 10.1016/j.envpol.2021.118407, 2022.

924 Verbrugge, F. H., Tang, W. H., and Hazen, S. L.: Protein carbamylation and
925 cardiovascular disease, *Kidney International*, 88, 474-478, 10.1038/ki.2015.166,
926 2015.

927 Veres, P. R., Roberts, J. M., Cochran, A. K., Gilman, J. B., Kuster, W. C., Holloway, J.
928 S., Graus, M., Flynn, J., Lefer, B., Warneke, C., and de Gouw, J.: Evidence of rapid
929 production of organic acids in an urban air mass, *Geophysical Research Letters*, 38,
930 L17807, 10.1029/2011gl048420, 2011.

931 Wang, Z., Nicholls, S. J., Rodriguez, E. R., Kummu, O., Horkko, S., Barnard, J.,
932 Reynolds, W. F., Topol, E. J., DiDonato, J. A., and Hazen, S. L.: Protein
933 carbamylation links inflammation, smoking, uremia and atherogenesis, *Nature*
934 *medicine*, 13, 1176-1184, 10.1038/nm1637, 2007.

935 Wang, Z., Yuan, B., Ye, C., Roberts, J., Wisthaler, A., Lin, Y., Li, T., Wu, C., Peng, Y.,
936 Wang, C., Wang, S., Yang, S., Wang, B., Qi, J., Wang, C., Song, W., Hu, W., Wang,
937 X., Xu, W., Ma, N., Kuang, Y., Tao, J., Zhang, Z., Su, H., Cheng, Y., Wang, X., and
938 Shao, M.: High Concentrations of Atmospheric Isocyanic Acid (HNCO) Produced
939 from Secondary Sources in China, *Environmental Science & Technology*, 54, 11818-
940 11826, 10.1021/acs.est.0c02843, 2020.

941 Wentzell, J. J., Liggio, J., Li, S. M., Vlasenko, A., Staebler, R., Lu, G., Poitras, M. J.,
942 Chan, T., and Brook, J. R.: Measurements of gas phase acids in diesel exhaust: a
943 relevant source of HNCO?, *Environmental Science & Technology*, 47, 7663-7671,
944 10.1021/es401127j, 2013.

945 Woodward-Massey, R., Taha, Y. M., Moussa, S. G., and Osthoff, H. D.: Comparison of
946 negative-ion proton-transfer with iodide ion chemical ionization mass spectrometry
947 for quantification of isocyanic acid in ambient air, *Atmospheric Environment*, 98,
948 693-703, 10.1016/j.atmosenv.2014.09.014, 2014.

949 Wren, S. N., Liggio, J., Han, Y., Hayden, K., Lu, G., Mihele, C. M., Mittermeier, R. L.,
950 Stroud, C., Wentzell, J. J. B., and Brook, J. R.: Elucidating real-world vehicle
951 emission factors from mobile measurements over a large metropolitan region: a focus
952 on isocyanic acid, hydrogen cyanide, and black carbon, *Atmospheric Chemistry and*
953 *Physics*, 18, 16979-17001, 10.5194/acp-18-16979-2018, 2018.

954 Wu, C., Wang, C., Wang, S., Wang, W., Yuan, B., Qi, J., Wang, B., Wang, H., Wang, C.,
955 Song, W., Wang, X., Hu, W., Lou, S., Ye, C., Peng, Y., Wang, Z., Huangfu, Y., Xie,
956 Y., Zhu, M., Zheng, J., Wang, X., Jiang, B., Zhang, Z., and Shao, M.: Measurement

957 report: Important contributions of oxygenated compounds to emissions and
 958 chemistry of volatile organic compounds in urban air, *Atmos. Chem. Phys.*, 20,
 959 14769-14785, <https://doi.org/10.5194/acp-20-14769-2020>, 2020.

960 Yan, Y., Wang, S., Zhu, J., Guo, Y., Tang, G., Liu, B., An, X., Wang, Y., and Zhou, B.:
 961 Vertically increased NO₃ radical in the nocturnal boundary layer, *Science of The*
 962 *Total Environment*, 763, 142969, <https://doi.org/10.1016/j.scitotenv.2020.142969>,
 963 2021.

964 Yáñez-Serrano, A. M., Nölscher, A. C., Bourtsoukidis, E., Gomes Alves, E., Ganzeveld,
 965 L., Bonn, B., Wolff, S., Sa, M., Yamasoe, M., Williams, J., Andreae, M. O., and
 966 Kesselmeier, J.: Monoterpene chemical speciation in a tropical rainforest: variation
 967 with season, height, and time of day at the Amazon Tall Tower Observatory (ATTO),
 968 *Atmospheric Chemistry and Physics*, 18, 3403-3418, 10.5194/acp-18-3403-2018,
 969 2018.

970 Yao, L., Wang, M. Y., Wang, X. K., Liu, Y. J., Chen, H. F., Zheng, J., Nie, W., Ding, A.
 971 J., Geng, F. H., Wang, D. F., Chen, J. M., Worsnop, D. R., and Wang, L.: Detection
 972 of atmospheric gaseous amines and amides by a high-resolution time-of-flight
 973 chemical ionization mass spectrometer with protonated ethanol reagent ions,
 974 *Atmospheric Chemistry and Physics*, 16, 14527-14543, 10.5194/acp-16-14527-2016,
 975 2016.

976 Yu, S.: Role of organic acids (formic, acetic, pyruvic and oxalic) in the formation of
 977 cloud condensation nuclei (CCN): a review, *Atmospheric Research*, 53, 185-217,
 978 [https://doi.org/10.1016/S0169-8095\(00\)00037-5](https://doi.org/10.1016/S0169-8095(00)00037-5), 2000.

979 Yuan, B., Koss, A. R., Warneke, C., Coggon, M., Sekimoto, K., and de Gouw, J. A.:
 980 Proton-Transfer-Reaction Mass Spectrometry: Applications in Atmospheric Sciences,
 981 *Chemical reviews*, 117, 13187-13229, 10.1021/acs.chemrev.7b00325, 2017.

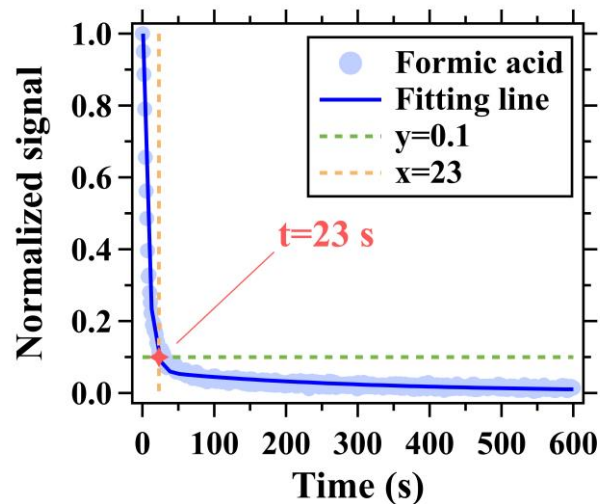
982 Yuan, B., Shao, M., de Gouw, J., Parrish, D. D., Lu, S., Wang, M., Zeng, L., Zhang, Q.,
 983 Song, Y., Zhang, J., and Hu, M.: Volatile organic compounds (VOCs) in urban air:
 984 How chemistry affects the interpretation of positive matrix factorization (PMF)
 985 analysis, *Journal of Geophysical Research: Atmospheres*, 117, n/a-n/a,
 986 10.1029/2012jd018236, 2012.

987 Yuan, B., Veres, P. R., Warneke, C., Roberts, J. M., Gilman, J. B., Koss, A., Edwards,
 988 P. M., Graus, M., Kuster, W. C., Li, S. M., Wild, R. J., Brown, S. S., Dubé, W. P.,
 989 Lerner, B. M., Williams, E. J., Johnson, J. E., Quinn, P. K., Bates, T. S., Lefer, B.,
 990 Hayes, P. L., Jimenez, J. L., Weber, R. J., Zamora, R., Ervens, B., Millet, D. B.,
 991 Rappenglück, B., and de Gouw, J. A.: Investigation of secondary formation of formic
 992 acid: urban environment vs. oil and gas producing region, *Atmospheric Chemistry*
 993 *and Physics*, 15, 1975-1993, 10.5194/acp-15-1975-2015, 2015.

994 Zhao, R., Yin, B., Zhang, N., Wang, J., Geng, C., Wang, X., Han, B., Li, K., Li, P., Yu,
 995 H., Yang, W., and Bai, Z.: Aircraft-based observation of gaseous pollutants in the
 996 lower troposphere over the Beijing-Tianjin-Hebei region, *Science of The Total*
 997 *Environment*, 773, 144818, 10.1016/j.scitotenv.2020.144818, 2021.

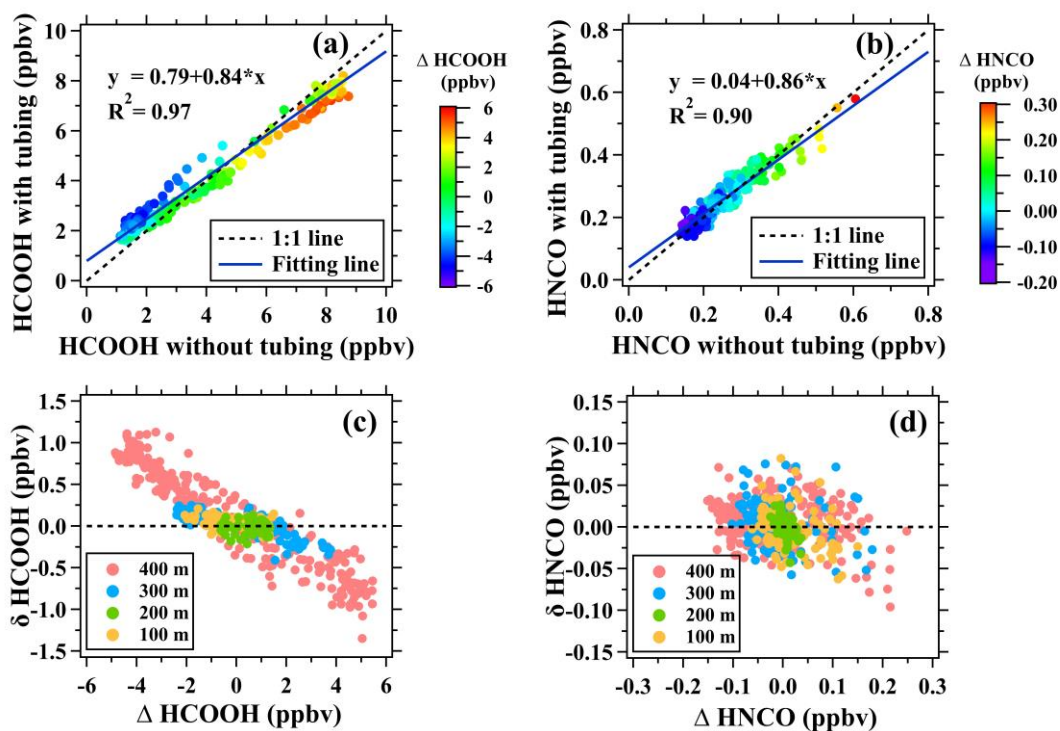
998 Zhao, R., Lee, A. K. Y., Wentzell, J. J. B., McDonald, A. M., Toom-Sauntry, D., Leitch,

999 W. R., Modini, R. L., Corrigan, A. L., Russell, L. M., Noone, K. J., Schroder, J. C.,
1000 Bertram, A. K., Hawkins, L. N., Abbatt, J. P. D., and Liggio, J.: Cloud partitioning
1001 of isocyanic acid (HNCO) and evidence of secondary source of HNCO in ambient
1002 air, *Geophysical Research Letters*, 41, 6962-6969, 10.1002/2014gl061112, 2014.
1003 Zhu, B., Han, Y., Wang, C., Huang, X., Xia, S., Niu, Y., Yin, Z., and He, L.:
1004 Understanding primary and secondary sources of ambient oxygenated volatile
1005 organic compounds in Shenzhen utilizing photochemical age-based parameterization
1006 method, *Journal of Environmental Sciences (China)*, 75, 105-114,
1007 10.1016/j.jes.2018.03.008, 2019.
1008



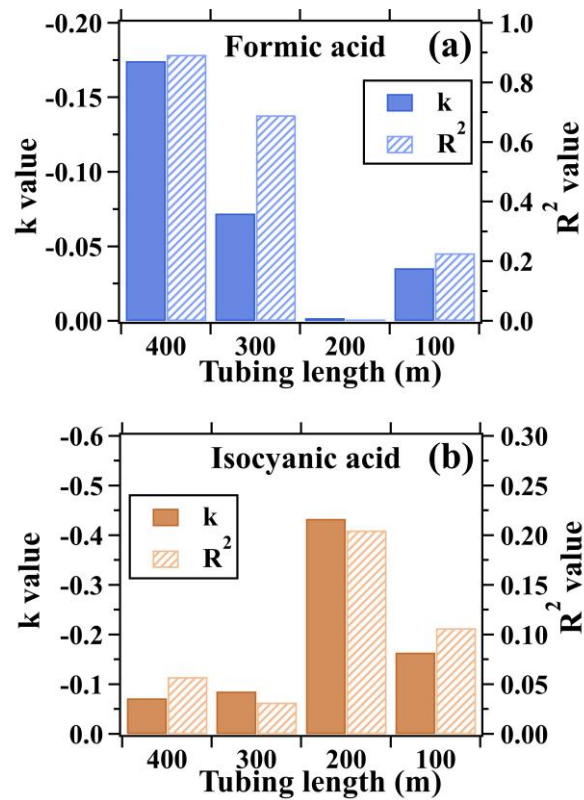
1009

1010 **Figure 1.** Depassivation curves of formic acid signal measured by I^- ToF-CIMS for the
1011 400 m long tubing at the flow rate of 13 SLPM. Ion signals were normalized to those
1012 measured at the start time (0 s) of the step-function change.



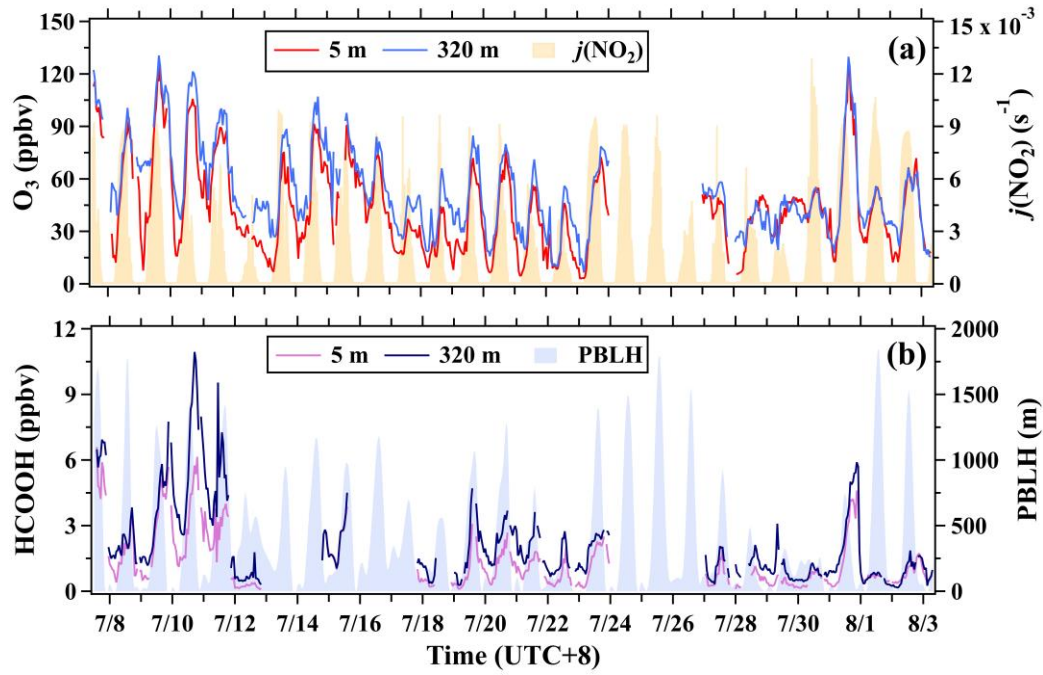
1013

1014 **Figure 2.** Assessment of long tubes in measuring formic and isocyanic acids in ambient
 1015 air. (a-b) Scatterplots of mixing ratios of formic and isocyanic acids measured with the
 1016 400 m long tube versus those measured without the long tube. (c-d) Scatterplots of
 1017 Δ [HCOOH] versus δ [HCOOH] and scatterplots of Δ [HNCO] versus δ [HNCO] for
 1018 the 100, 200, 300, and 400 m tubes.



1019

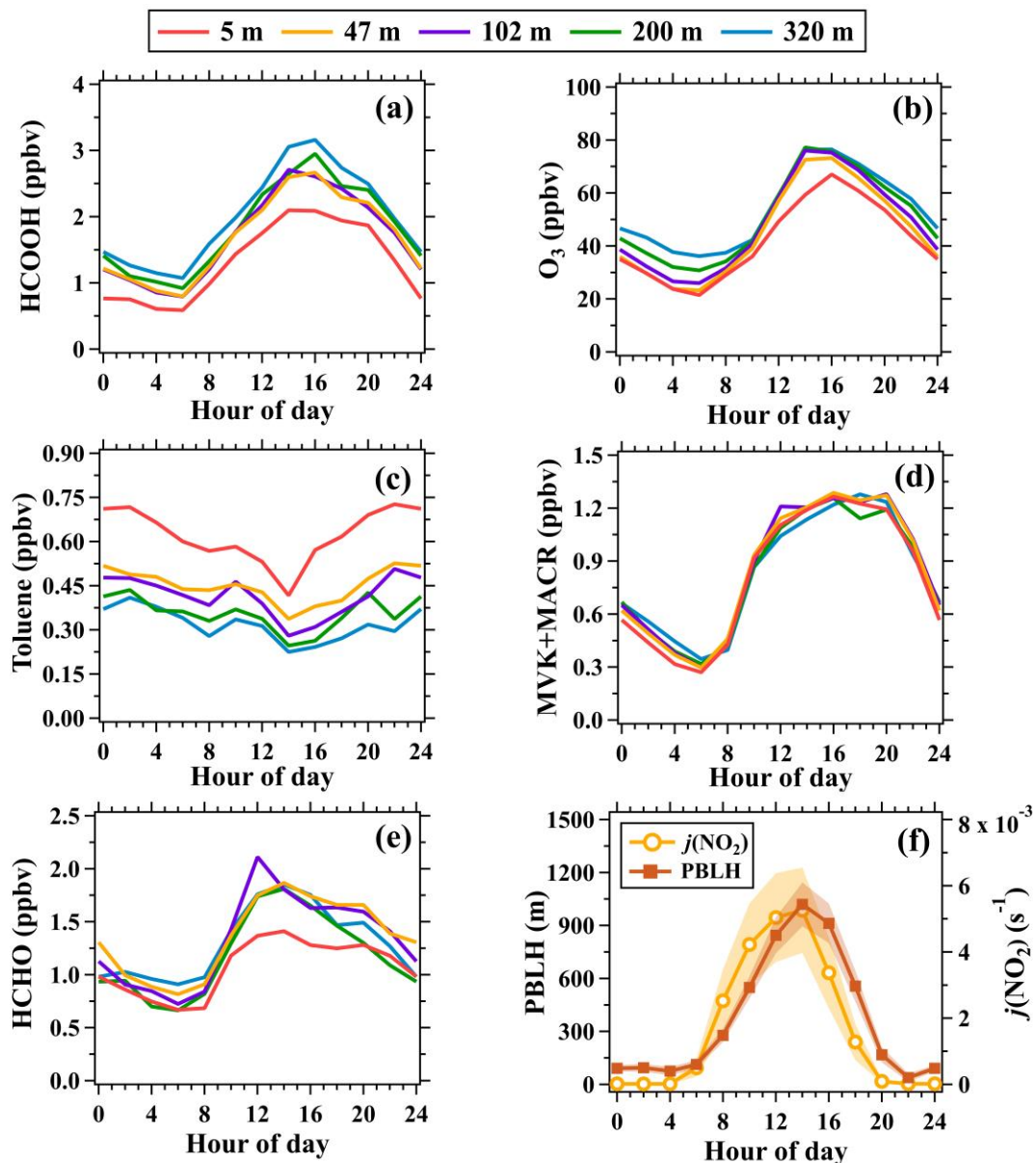
1020 **Figure 3.** Linear fitting parameters (namely k and R^2) for (a) $\Delta[HCOOH]$ versus
 1021 $\delta[HCOOH]$ and (b) $\Delta[HNCO]$ versus $\delta[HNCO]$. The scatterplots are shown in
 1022 Figure 2. k and R^2 are the slope and determination coefficient of the linear fitting lines,
 1023 respectively.



1024

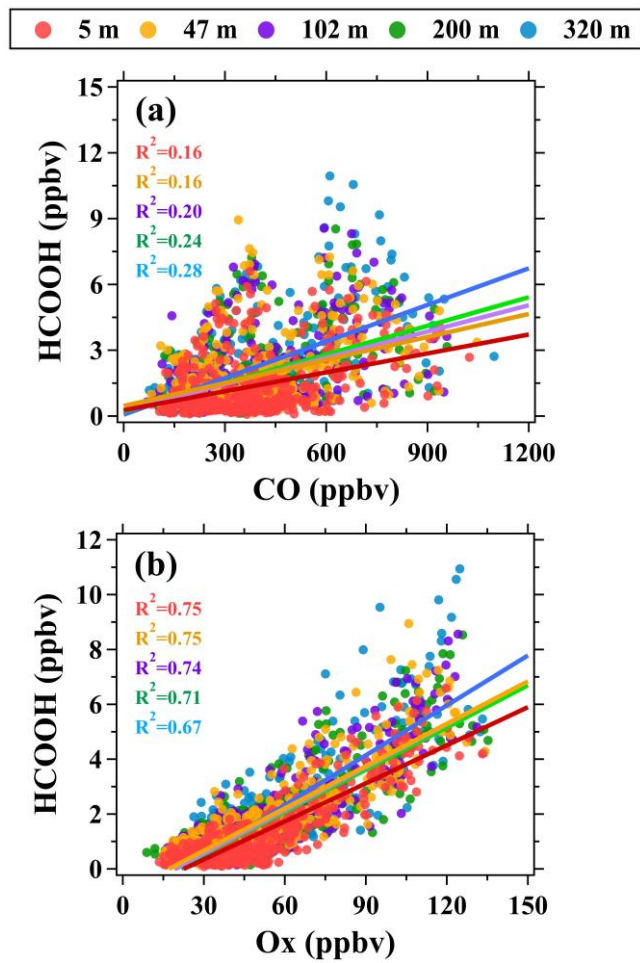
1025 **Figure 4.** Time series of (a) O₃ (5 and 320 m), $j(\text{NO}_2)$, (b) formic acid (5 and 320 m),

1026 and planetary boundary layer height (PBLH) during the campaign.



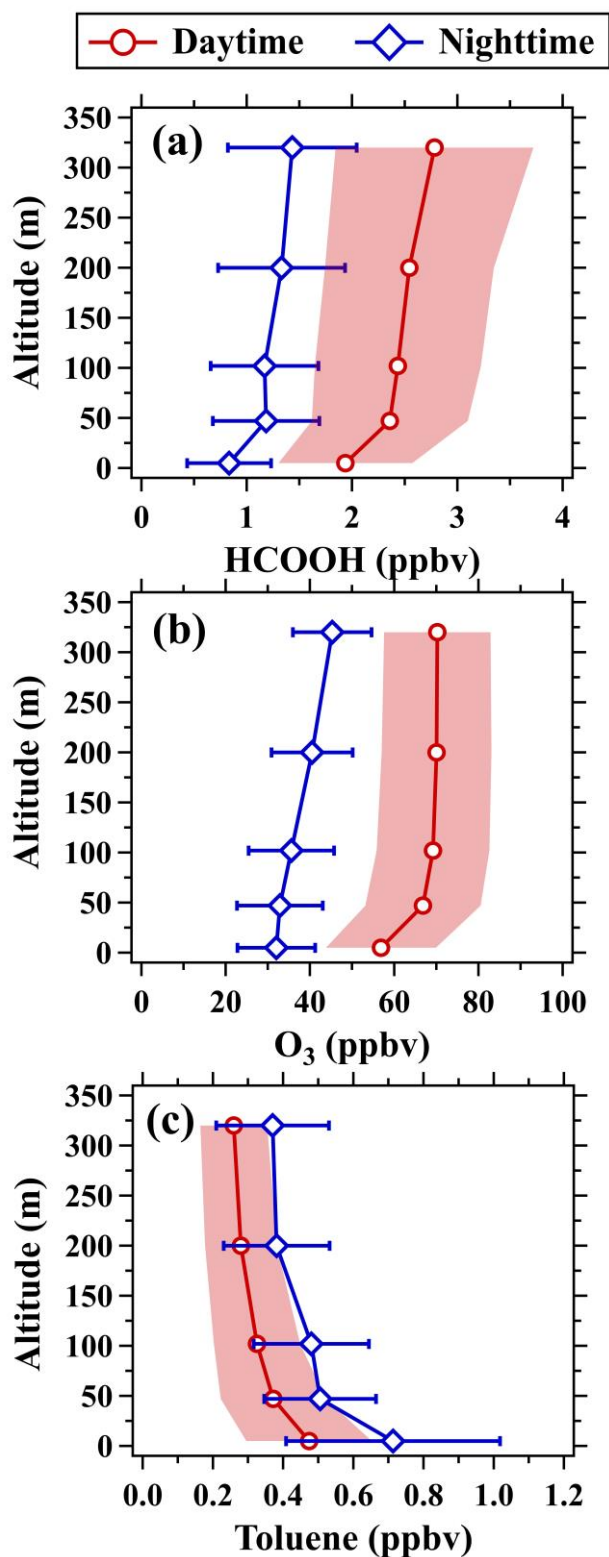
1027

1028 **Figure 5.** Average diurnal variations in mixing ratios of (a) formic acid, (b) O₃, (c)
 1029 toluene, (d) MVK+MACR, (e) formaldehyde at the five inlet heights and (f) PBLH and
 1030 $j(\text{NO}_2)$. The shaded areas in panel (f) are half of the standard deviations.



1031

1032 **Figure 6.** Scatter plots of (a) formic acid versus CO and (b) formic acid versus Ox at
 1033 different altitudes during the campaign.

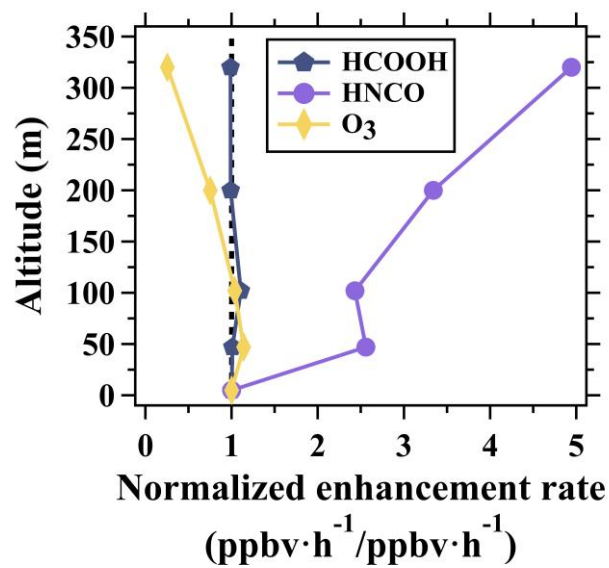


1034

1035 **Figure 7.** Vertical profiles of (a) formic acid, (b) O₃, and (c) toluene in daytime (11:00-

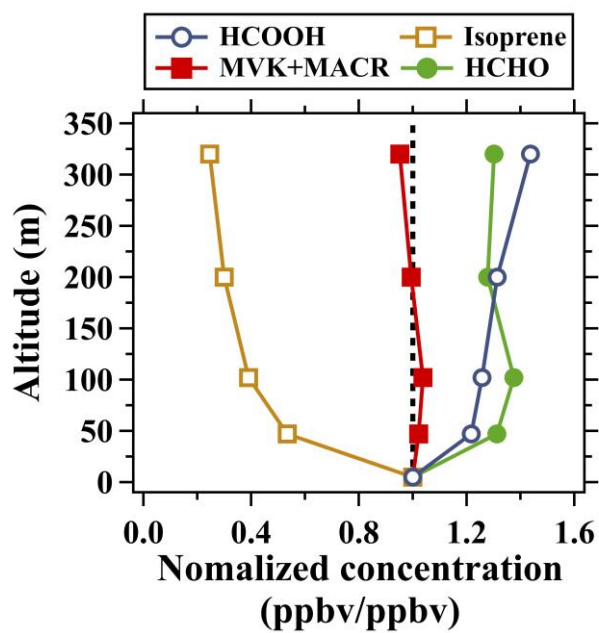
1036 16:00 LT) and nighttime (22:00-5:00 LT). The shaded areas and error bars are half of

1037 the standard deviations.



1038

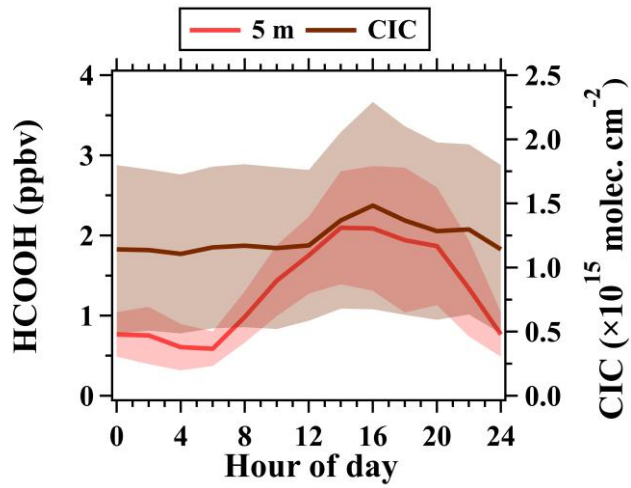
1039 **Figure 8.** Normalized vertical profiles of the enhancement rate of ozone, formic acid,
 1040 and isocyanic acid between 6:00-10:00 LT averaged over the whole campaign.
 1041 Enhancement rate of the species at different altitudes were normalized to those at 5 m.
 1042 The dotted line indicates the normalized enhancement rate of 1.



1043

1044 **Figure 9.** Normalized vertical profiles of formic acid, isoprene, formaldehyde, MVK
 1045 and MACR in daytime (11:00-16:00 LT) averaged over the whole campaign. Mixing
 1046 ratios of the species at different altitudes were normalized to those at 5 m. The dotted
 1047 line indicates the normalized concentration of 1.

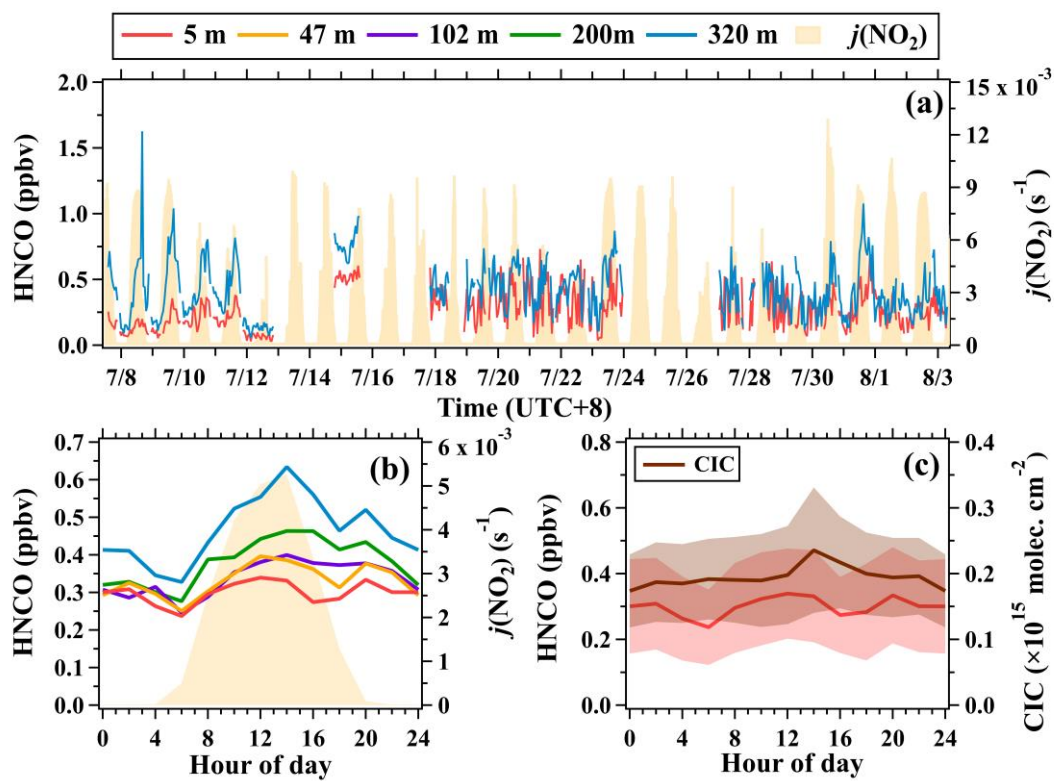
1048



1049

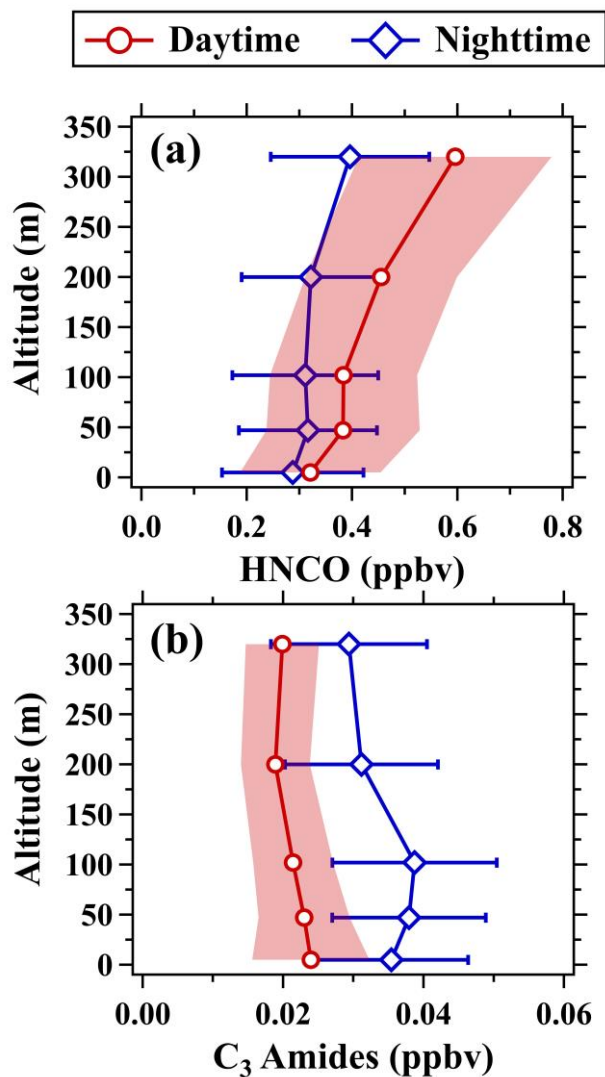
1050 **Figure 10.** Average diurnal variations in mixing ratios (5 m) and CICs of formic acid

1051 during the field campaign; The shaded areas are half of the standard deviations.



1052

1053 **Figure 11.** (a) Time series of isocyanic acid (5 and 320 m) and $j(\text{NO}_2)$. (b) Average
 1054 diurnal variations in isocyanic acid at 5, 47, 102, 200, and 320 m. (c) Average diurnal
 1055 variations in mixing ratios (5 m) and CICs of isocyanic acid during the campaign; The
 1056 shaded areas in panel (c) are half of the standard deviations.



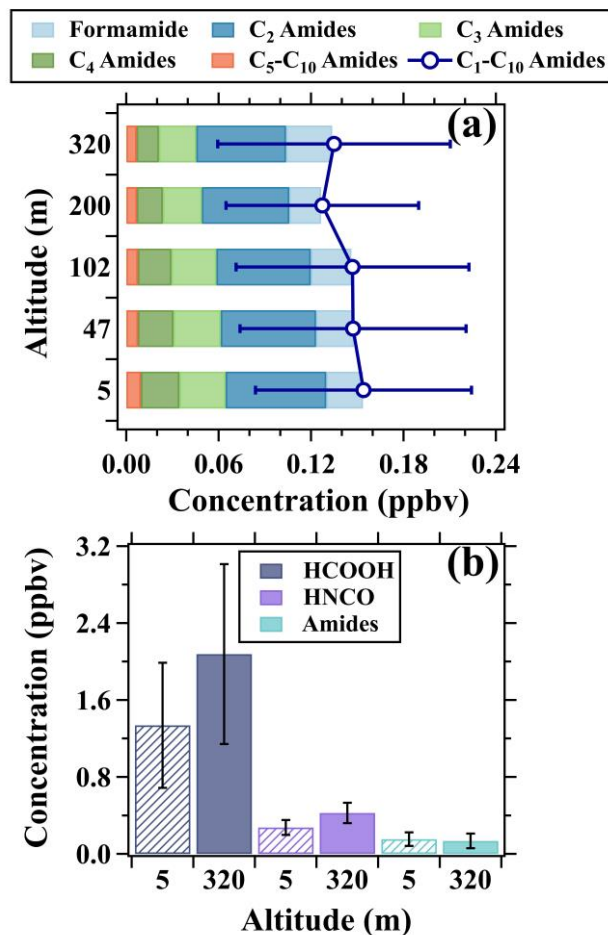
1057

1058 **Figure 12.** Vertical profiles of (a) isocyanic acid and (b) C₃ amides in daytime (11:00-

1059 16:00 LT) and nighttime (22:00-5:00 LT). The shaded areas and error bars are half of

1060 the standard deviations.

1061



1062

1063 **Figure 13.** (a) Vertical variations in composition and concentrations of amides. (b)
 1064 Concentration comparison of formic acid, isocyanic acid, and amides between 5 and
 1065 320 m. The data in both (a) and (b) was the average results of the whole campaign. The
 1066 patterns of the bars are used to distinguish the average concentration of the species at
 1067 the two heights.